

St. John's University

**St. John's Scholar**

---

Theses and Dissertations

---

2021

**DOUBLE-COATED BIODEGRADABLE POLY (BUTYL  
CYANOACRYLATE) NANOPARTICULATE DELIVERY SYSTEMS FOR  
BRAIN TARGETING OF DOXORUBICIN VIA ORAL  
ADMINISTRATION**

Neeraj Kaushal

Follow this and additional works at: [https://scholar.stjohns.edu/theses\\_dissertations](https://scholar.stjohns.edu/theses_dissertations)



Part of the [Pharmacy and Pharmaceutical Sciences Commons](#)

---

DOUBLE-COATED BIODEGRADABLE POLY (BUTYL  
CYANOACRYLATE) NANOPARTICULATE DELIVERY SYSTEMS FOR  
BRAIN TARGETING OF DOXORUBICIN VIA ORAL ADMINISTRATION

A dissertation submitted in partial fulfillment  
of the requirements for the degree of

DOCTOR OF PHILOSOPHY

to the faculty of the

DEPARTMENT OF GRADUATE DIVISION

of

COLLEGE OF PHARMACY AND HEALTH SCIENCES

at

ST. JOHN'S UNIVERSITY

New York

by

Neeraj Kaushal

Date Submitted 03/26/2021

Date Approved 03/26/2021

---

Neeraj Kaushal

---

Dr. Senshang Lin

**© Copyright by Neeraj Kaushal 2021**

**All Rights Reserved**

## ABSTRACT

### DOUBLE-COATED BIODEGRADABLE POLY(BUTYL CYANOACRYLATE) NANOPARTICULATE DELIVERY SYSTEMS FOR BRAIN TARGETING OF DOXORUBICIN VIA ORAL ADMINISTRATION

Neeraj Kaushal

Primary brain cancer cells grow within the brain or cancer cells can metastasize from different sites of the body into the brain. The major hurdle in the treatment of brain cancer is the presence of the blood-brain barrier (BBB). Additionally, acquired multidrug-resistant (MDR) impedes the success of long-term chemotherapy. Therefore, the objective of this investigation is to evaluate the brain targeting potential of orally administered poly(butyl cyanoacrylate) nanoparticulate delivery systems (PBCA-NPDS), double-coated with Tween 80 and polyethylene glycol (PEG) 20000 for brain delivery of doxorubicin, that does not cross the BBB by itself. And, evaluate the MDR reversal potential of PBCA-NPDS. Doxorubicin-loaded PBCA-NPDS were prepared by the anionic polymerization method and were successively double-coated with Tween 80 and PEG 20000 in varied concentrations. Brain uptake study of double-coated doxorubicin-loaded PBCA-NPDS using bEnd.3 cell line suggested the role of clathrin-mediated endocytosis in the uptake of double-coated doxorubicin-loaded PBCA-NPDS. When Transwell® permeable supports were used, significant transport of doxorubicin across the cell monolayer was observed by the double-coated formulations, in comparison to doxorubicin solution ( $p < 0.05$ ). Significant accumulation of doxorubicin in brain was achieved after oral administration of double-coated doxorubicin-loaded PBCA-NPDS in rats ( $p < 0.05$ ). Furthermore, simultaneously analyzing the pharmacokinetic data obtained after intravenous and oral administrations, revealed the role of lymphatics in absorption

of double-coated doxorubicin-loaded PBCA-NPDS. When MDR reversal potential of PBCA-NPDS was evaluated by cell uptake in P-gp overexpressing cell line, significant uptake of doxorubicin was mediated by double-coated doxorubicin-loaded PBCA-NPDS ( $p < 0.05$ ). These results were verified by MTT assay in P-gp or BCRP overexpressing cell lines. MTT assays revealed that double-coated doxorubicin-loaded PBCA-NPDS significantly potentiated the sensitivity of doxorubicin in P-gp overexpressing cells, in comparison to doxorubicin solution, single-, and un-coated doxorubicin-loaded PBCA-NPDS ( $p < 0.05$  in all case), respectively. Further increase in concentration of Tween 80, significantly enhanced the sensitivity of doxorubicin in BCRP overexpressing cell line, in comparison to single- and double-coated doxorubicin-loaded PBCA-NPDS (with lower concentration of Tween 80) ( $p < 0.05$  in all case). Hence, it could be concluded that double-coated doxorubicin loaded PBCA-NPDS could be used for brain targeting of doxorubicin administered orally and overcome MDR.

## DEDICATION

*The thesis is dedicated to my family for their endless love, support, and  
encouragement*

## ACKNOWLEDGEMENT

I am grateful to The Almighty God for guiding me to accomplish this journey. I would like to express my sincere thanks and profound gratitude to my mentor, Dr. Senshang Lin, for his constant motivation and guidance during the course of my research. It was his patience, flexibility, directions, and most importantly his course works that ingrained me with the idea of critical thinking, work independently, analyze, and argue critically. His encouragement to think beyond the textbook gave me a fresh perspective towards not only research but also life as a whole.

I also take this opportunity to thank Dr. B. Rohera, Dr. Z.S.Chen, Dr. V. Gupta, and Dr. K. Patel for serving on my committee and to giving me valuable suggestions from time to time and helping me with my dissertation work. I acknowledge the Department of Pharmaceutical sciences, Dr. V. Korlipara, Mery and College of Pharmacy and Health Sciences at St. John's University, Dr. Gillespie, and Arlene for providing me with the financial assistance and other facilities.

My PhD journey would have not been so joyful without good friends, I would like to thank Khushboo, Anuja, Ankit, Zhangjie, and Kanyaphat (Wow) for their constructive comments, support, shared joy, and their constant motivation throughout my research. I would like to specially thank Khushboo for her unconditional support and sharing her knowledge during animal studies. I cannot thank enough my family for the sacrifices they have made and the dreams they had to let go, just to see me progress in career and life. Thank you for believing in

me and being the constant driving force throughout this journey. I would like to specially thank my wife and kids (Neil and Gauri), for their unconditional love and support. During this journey my kids thought me some wonderful life lessons of being happy for no reason and resilience. I could not have reached so far without all of you.



## TABLE OF CONTENTS

DEDICATION.....	ii
ACKNOWLEDGEMENT.....	iii
LIST OF TABLES.....	ix
LIST OF FIGURES.....	x
1. Introduction.....	x
2. Literature review.....	2
2.1. Brain tumors and doxorubicin.....	2
2.2. Oral absorption of surface modified nanoparticles.....	3
2.3. Brain targeting of surface modified nanoparticles.....	8
2.4. Fabrication of nanoparticles.....	11
2.5. Fabrication of oral double-coated nanoparticles for brain delivery.....	14
2.6. Characterization of nanoparticles.....	16
2.6.1. Physicochemical characterization.....	16
2.6.2. Degradation pathway of polymeric nanoparticles.....	18
2.6.3. Drug release.....	18
3. Research objectives and specific aims.....	20
4. Materials and methods.....	21
4.1. Materials.....	21

4.2. Analysis of doxorubicin .....	22
4.2.1. UV-Vis spectroscopy method .....	22
4.2.2. Fluorescence spectroscopy method (plate-reader method) .....	22
4.2.3. Fluorescent microscopy method.....	23
4.3. Fabrication of double-coated doxorubicin-loaded poly(butyl cyanoacrylate) nanoparticles delivery systems (PBCA-NPDS) .....	24
4.3.1. Doxorubicin-loaded PBCA-NPDS.....	24
4.3.2. Single-coating of doxorubicin-loaded PBCA-NPDS .....	26
4.3.3. Double-coating of doxorubicin-loaded PBCA-NPDS .....	26
4.4. In vitro evaluation of double-coated doxorubicin-loaded PBCA-NPDS .....	27
4.4.1. Particle size and zeta potential .....	27
4.4.2. Entrapment efficiency .....	28
4.4.3. In vitro drug release kinetics .....	28
4.4.3.1. Screening of dialysis membrane bags .....	28
4.4.3.2. In vitro release study .....	29
4.4.4. Drug-leakage in various simulated mediums .....	30
4.4.4.1. Fasted state simulated intestinal fluids (FaSSIF) .....	30
4.4.4.2. Serum .....	30
4.5. In vitro model to elucidate the brain uptake mechanism .....	31
4.5.1. Uptake mechanism elucidation using specific inhibitors as a pretreatment.....	31


4.5.2. Permeability screening study .....	32
4.6. In vivo performance of double-coated doxorubicin loaded PBCA-NPDS .....	33
4.6.1. Biodistribution study .....	33
4.6.2. Pharmacokinetic study .....	33
4.7. In vitro cell culture studies .....	34
4.7.1. Intracellular accumulation study of various in doxorubicin-loaded PBCA-NPDS in SW620, AD300 and bEnd.3 cell lines .....	34
4.7.2. Cytotoxicity determination of various doxorubicin-loaded PBCA-NPDS to evaluate their P-gp and BCRP efflux transporter inhibition potential .....	35
4.8. Data analysis .....	35
4.8.1. Pharmacokinetic data analysis .....	35
4.8.2. Statistical analysis .....	37
5. Results and discussion .....	37
5.1. Analytical methodology .....	37
5.2. Fabrication and characterization of double-coated doxorubicin loaded PBCA- NPDS.....	38
5.3. In vitro drug release.....	41
5.3.1. Screening of dialysis membrane .....	41
5.3.2. In vitro drug release study of various doxorubicin loaded PBCA-NPDS.....	42
5.4. Drug leakage study in FaSSIF and serum .....	43

5.5. In vitro model to elucidate the brain uptake mechanism .....	44
5.5.1. Uptake mechanism elucidation using specific inhibitors as a pretreatment.....	44
5.5.2. Permeability screening study .....	46
5.6. Biodistribution and pharmacokinetic studies in rats .....	47
5.6.1. Biodistribution studies.....	47
5.6.2. Pharmacokinetic studies.....	49
5.7. In vitro cell culture studies .....	50
6. Conclusion.....	54
7. Tables.....	56
8. Figures .....	60
9. References .....	82

## LIST OF TABLES

Table 1: Physiochemical characterization methods for nanoparticles .....	56
Table 2: Formulation codes and characteristics of various doxorubicin-loaded PBCA-NPDS. Data presented as mean $\pm$ standard deviation, n = 3.....	57
Table 3: The cytotoxic effect of doxorubicin and double-coated doxorubicin-loaded PBCA-NPDS on SW620 and AD300 cell lines.....	58
Table 4: The cytotoxic effect of doxorubicin and double-coated doxorubicin-loaded PBCA-NPDS on H460 and MX20 cell lines.....	59

## LIST OF FIGURES

- Figure 1: Schematic representation of three possible mechanisms of gastrointestinal uptake of surface modified poly(butyl cyanoacrylate) nanoparticles (PBCA-NPDS). Represents surface modified PBCA-NPDS: (a) intracellular uptake (*via* intra-epithelial lymphatics, IELs); (b) intracellular/paracellular uptake; (c) uptake *via* the M-cells and Peyer's patches in the gut lumen. Adapted from reference (1) with modifications. .... 60
- Figure 2: Schematic representation pathway of doxorubicin delivery to the brain facilitated by double-coated doxorubicin-loaded PBCA-NPDS after oral administration: (a) doxorubicin efflux in the lumen facilitated by the P-gp receptor in the duodenum following either intracellular and/or paracellular uptake by the duodenum, (b) uptake of double-coated doxorubicin-loaded PBCA-NPDS via the M-cells of the Peyer's patches of the ileum, and (c) LDL-receptor mediated transcytosis of the double-coated doxorubicin-loaded PBCA-NPDS from blood lumen into the brain..... 61
- Figure 3: Schematic representation of nanoparticle formulation. (A) doxorubicin-loaded PBCA-NPDS (core), (B) Tween 80 overcoated nanoparticles, and (C) Tween 80 and PEG 20000 overcoated nanoparticles. Adapted from reference (67) with modifications..... 62
- Figure 4: Calibration curve of doxorubicin assayed by the UV-Vis spectroscopy method ( $R^2 = 0.9996$ ,  $n = 6$ ). ..... 63
- Figure 5: Calibration curve of doxorubicin assayed by the fluorescence spectroscopy (plate-reader method) spiked in various medium ( $R^2 > 0.995$  in each case ,  $n = 6$ )..... 64
- Figure 6: Fluorescence microscopy images of cells for method selection. A) cell nuclei stained DAPI, B) cells treated with free doxorubicin, exhibiting characteristic red

fluorescence associated with doxorubicin within the cell, and C) merged image of the cells is depicted by an arrow. (Scale bar: 10 $\mu$ m). .....	65
Figure 7: $^1\text{H}$ NMR of spectrums of a) doxorubicin-loaded PBCA-NPDS, and b) free doxorubicin in DMSO- $d_6$ . Arrow shows a characteristics peak for the protons associated with amine and aliphatic carbon atom (boxed in the chemical structure). .....	66
Figure 8: Comparison of diffusion profiles of free doxorubicin using different MWCO dialysis membranes in the release medium at $37^\circ \pm 0.5^\circ\text{C}$ , 100-120 rpm. (Data are presented as mean $\pm$ standard deviation, n = 3). .....	67
Figure 9: In vitro drug release profiles of various doxorubicin-loaded PBCA-NPDS (Data presented as mean $\pm$ standard deviation, n = 3). .....	68
Figure 10: % Doxorubicin leakage from various doxorubicin-loaded PBCA-NPDS after 12 hours incubation period in a) FaSSIF, and b) Serum at $37^\circ \pm 0.5^\circ\text{C}$ and 100–120 rpm. (Data presented as mean $\pm$ standard deviation, n = 3). .....	69
Figure 11: The in vitro model in which bEnd.3 cells were subjected to various inhibitors as pretreatments, and then followed with treatment of formulation T2P2 or doxorubicin solution for additional 3 hours of cell incubation for elucidation of the brain uptake mechanism (data presented as mean $\pm$ standard deviation, n = 6). .....	70
Figure 12: Apparent permeability ( $P_{\text{app}}$ ) after transport experiment of formulation T2P2 or doxorubicin solution across bEnd.3 cells monolayer after 2 hours incubation period (data presented as mean $\pm$ standard deviation, n = 3). *p = 0.003 and #p = 0.004 of doxorubicin permeation (higher) and efflux (lower) mediated by formulation T2P2, from apical to basolateral and basolateral to apical side, respectively, in comparison to doxorubicin solution. ....	71

Figure 13: Biodistribution of doxorubicin in a) serum, b) brain, and c) liver from formulation T2P2 after intravenous administration (group 1) and oral administration (groups 2-3), in comparison to oral doxorubicin solution (data present mean  $\pm$  standard deviation, n = 2). \*p = 0.017 in comparison to 1 hour,..... 72

Figure 14: Simultaneous model fitting of pooled doxorubicin serum concentration-time profiles after intravenous administration of formulation T2P2 (27 mg/kg), respectively, with a) oral administration of T2P2 (50 mg/kg), b) oral administration of T2P2 (70 mg/kg), and c) oral administration of doxorubicin solution (70 mg/kg). ..... 73

Figure 15: Fluorescence associated with intracellular accumulation of doxorubicin within human colon adenocarcinoma cell line SW620, following treatment with, (a) T0P0, (b) T0P1, (c) T1P0, (d) T1P1, (e) T1P2 (f) T2P1, (g) T2P2, (h) Free doxorubicin, and (i) No treatment. Note: Arrows represent the accumulation of doxorubicin in the nucleus. (Magnification: 40 $\times$ , Scale bar: 10  $\mu$ m). ..... 74

Figure 16: The values of calculated corrected total cell fluorescence intensity within SW620 cells, based on the outcomes shown in Figure 15 (data presented as mean  $\pm$  standard deviation, number of cells counted = 50, \*p = < 0.001). ..... 75

Figure 17: Fluorescence detection upon the intracellular accumulation of doxorubicin in doxorubicin-resistant human colon adenocarcinoma cell line AD300, following treatment with, (a) T0P0, (b) T0P1, (c) T1P0, (d) T1P1, (e) T1P2 (f) T2P1, (g) T2P2, (h) Free doxorubicin, and (i) No treatment. Arrows represent the accumulation of doxorubicin in the nucleus. (Magnification: 40 $\times$ , Scale bar: 10  $\mu$ m). ..... 76



Figure 18: The values of calculated corrected total cell fluorescence intensity within AD300 cells, based on the outcomes shown in Figure 17 (data presented as mean  $\pm$  standard deviation, number of cells counted = 30, \*p = < 0.001). ..... 77

Figure 19: Concentration dependent cytotoxicity profile obtained after treating SW620 cell lines with various doxorubicin-loaded PBCA-NPDS in comparison with free doxorubicin. Data presented as mean  $\pm$  standard deviation, and representative of three independent experiments in triplicate are shown. .... 78

Figure 20: Concentration dependent cytotoxicity profile obtained after treating AD300 cell line with various doxorubicin-loaded PBCA-NPDS in comparison with free doxorubicin. Data presented as mean  $\pm$  standard deviation, and representative of three independent experiments in triplicate are shown. .... 79

Figure 21: Concentration dependent cytotoxicity profile obtained after treating H460 cell line with various doxorubicin-loaded PBCA-NPDS in comparison with free doxorubicin. Data presented as mean  $\pm$  standard deviation, and representative of three independent experiments in triplicate are shown. .... 80

Figure 22: Concentration dependent cytotoxicity profile obtained after treating MX20 cell line with various doxorubicin-loaded PBCA-NPDS in comparison with free doxorubicin. Data presented as mean  $\pm$  standard deviation, and representative of three independent experiments in triplicate are shown. .... 81

## 1. Introduction

Malignant primary brain tumors are cancers that originate in the brain, which typically grow faster than benign tumors and aggressively invade the surrounding tissue. Although significant advances in terms of treatment using operative techniques, radiotherapy, and adjuvant chemotherapy have been made, the prognosis remains unfavorable. Even the adjuvant chemotherapy considered to be effective for treatments of these malignant tumors, such as temozolomide, the survival time of patients increases only marginally. In addition to this, such treatment regimen poses intense adverse effects to healthy cells. Hence, there is a need and opportunity for the growth of brain-targeted chemotherapy. However, achieving drug delivery to the brain, remains a challenging task, due to the presence of epithelia-like tight junction lining the brain capillary endothelium referred to as the blood-brain barrier (BBB) (2).

To facilitate drug delivery across the BBB, number of approaches such as, hyperosmotic disruption of the BBB (3), carrier systems like targeted antibodies (4), prodrugs (Temodar<sup>®</sup>), liposomes (5), and nanoparticles (6–8) have been explored. Among these approaches, surfactant coated nanoparticles have been reported successfully to deliver drug across the BBB (6,8–12). The nanoparticles coated with polysorbate 80 lead to the adsorption of apolipoprotein E from blood plasma on the surface of nanoparticles, which then seem to mimic low-density lipoprotein (LDL) which interacts with LDL receptor leading to their uptake by the endothelial cells lining the BBB (13,14).

## **2. Literature review**

### **2.1. Brain tumors and doxorubicin**

Brain tumors is a growth of tumor cells which occurs in the brain and can be very heterogenous groups of tumors. Upon their diagnosis, subsequent treatments such as radiation therapy or chemotherapy is initiated. Most of the chemotherapeutics are administered via intravenous bolus leading to initial rapid increase and subsequent decay of drug plasma concentrations (15). Tissue toxicity as well as poor biopharmaceutical properties (i.e., protein binding, first-pass metabolism, etc.) of these chemotherapeutic agents has led to number of attempts to develop more rational formulations for chemotherapy (16).

As described previously, poor oral bioavailability of doxorubicin can be partly attributed to over expression of the multidrug efflux transporter P-gp (13,14) specifically of the intestinal lumen. The general approach to resolve this problem would be to use P-gp inhibitors (i.e., cyclosporine A) to suppress elimination process. However, these inhibitors suppress body's immune system and may lead to drug-drug interaction ultimately leading to medical complications. Furthermore, these inhibitors are known to have their own side-effects making it more difficult to incorporate in the drug delivery systems along with chemotherapeutic agents (19). Recently, other approaches like advanced targeted drug delivery systems have been studied extensively offering potential alternatives to circumvent the aforementioned issues. Among which biodegradable polymeric nanoparticles with brain targeting efficiency seems to be one of the promising approaches for the development of oral chemotherapy with

high patient compliance as well as improved therapeutic efficacy and reduced adverse effects (7).

Among many properties of polymeric nanoparticles, the properties to control drug release at a desired rate and to allow the provision of surface modification with a homing device can be employed for desired drug release rate and targeting to the brain. Covalent attachment apolipoprotein AI and B-100 to albumin nanoparticles have shown to transport drug to the brain from systemic circulation. Nevertheless, these surface modified nanoparticles takes an advantage of the biochemical transport systems that are present in the BBB (20,21). Among these systems, the LDL-receptor and the transferrin transcytosis systems may be employed in the delivery of drugs.

## **2.2. Oral absorption of surface modified nanoparticles**

Gastrointestinal (GI) tract, including oral cavity, the stomach, the small intestine and the large intestine, is essentially a muscular tube lined by mucus membrane. The stomach is primarily a secretory organ and its gastric acid secretion and gastric emptying affect the drug absorption (22). However, these aspects of gastric physiology have little relevance when considering uptake of nanoparticulate delivery systems, owing to their size and specialized mechanism for their uptake. In contrast, when considering the absorption of nanoparticles from the intestine, specifically the small intestine, it is crucial to address the mechanism in ileum (23,24). A specialized mechanism for the absorption of solid lipid nutrients has been reported by Peyer. This absorption mechanism is related to gut-associated lymphoid tissue (GALT) in the ileum, which is known as the

Peyer's patches. Due to the similarity between solid lipid and nanoparticles, targeting nanoparticles to Peyer's patches as a port of entry of nanoparticles in the lymphatic circulation resulting in improved oral absorption. Schematic representation of the mechanisms of gastrointestinal uptake of surface modified nanoparticles [i.e., surface modified poly(butyl cyanoacrylate) nanoparticles] is shown in Figure 1. Furthermore, accumulation in Peyer's patches has been reported to be governed by nanoparticle surface properties and size. Wherein, the penetration being favored by nanoparticles with hydrophobic surfaces (25), and particle size less than about 300 nm as in the case of polystyrene particles after oral administration to rats (26).

Despite that three possibilities for uptake of nanoparticles have been suggested (Figure 1), the simultaneous occurrence of more than one pathway has been reported (27–30). The rapid appearance of orally administered nanoparticles in the circulation (10 minutes post-dosing) can only be explained by the paracellular pathway (28,31). Aprahamian et al. (28) reported the presence of nanoparticles in intercellular spaces (especially in larger defects of mucosa) between 10-15 minutes after intraluminal injection into the intestine of anesthetized Beagle dogs. After 15 minutes, the nanoparticles were already observable in the lamina propria in proximity of the basal membrane of the enterocytes. After 30 minutes, the nanoparticles were quite numerous at the internal surface of the vascular epithelium where they generally formed clusters and were noted to be in close contact with red cells. After 1 hour, very few

nanoparticles were found in the capillaries. Nanoparticles, although small in numbers, were also present in the lymph ducts in the core of the villus.

In one of the reported work, Sanders and Ashworth observed polystyrene nanoparticles of size of 220 nm within the epithelial cells of jejunum 1 hour after administration of these particles by oral gavage in rats, and after 2-4 hours the nanoparticles were observed in the interstices of the lamina propria and the lymphatics of mucosa (32). The observation of uptake of nanoparticles by the lining of the cells of the intestinal mucosa was also supported by the electron microscopic autoradiographic investigation by Kreuter et.al. (33). This intracellular uptake suggests an endocytic uptake mechanism, which was also proposed by Jani et. al. (29) as a secondary pathway for intestinal uptake polystyrene particle of diameter 100 nm.

M-Cells are classified as specialized epithelial cells which are generally found on the follicle-associated epithelium overlying Peyer's patches. Microscopically, the epithelial overlying these patches contain a small number of goblet cells, as a result, mucus secretion is reduced rendering M cell's surface as more conducive to antigen binding. For these reasons, M-cells may also be more easily accessible for nanoparticles (34). This can be validated by the observation by Jani et. al. (29) wherein they observed the uptake of polystyrol nanoparticles exhibiting fluorescent and ranging from a size range of 100 nm and 1 $\mu$ m by the Peyer's patches following oral gavage to mice daily for 10 days. The nanoparticles were found to be concentrated in the serosal side of the Peyer's patches and following a histological investigation revealed the translocation of

particles of size 1  $\mu\text{m}$  and smaller from the Peyer's patches to the mesenteric lymph nodes leading to the lymphatic system. In a comparison of radiolabeled ( $^{125}\text{I}$ ) labeled particles of sizes 100 nm and 1  $\mu\text{m}$ , smaller sized particles showed a higher uptake, with smaller particle being observed in liver and spleen, with no evidence for uptake of particles of sizes 3  $\mu\text{m}$  and higher by the gut (35).

As illustrated above, evidence for all three pathways exists. However, many researches have reported the simultaneous occurrence of more than one pathway for the uptake of nanoparticles by the GI tract (28–30,32). For example, Damgé et. al. (27) reported a preferential uptake of lipiodol-loaded nanoparticles via intercellular spaces between the enterocytes in the jejunum 10-15 minutes following oral administration to canine and rats. Wherein large quantities of particles passed through the M-cells of the ileum and were found to be in the intercellular spaces around the lymph nodes simultaneously. In addition to this, Scherer et. al. (36), in their *in vitro* diffusion experiment, observed by using laser confocal microscopy that fluorescence appeared in localized patches when fluorescein isothiocyanide (FITC) labeled nanoparticles were applied onto either porcine or rabbit small intestine, as compared to homogenous distribution over this tissue when FITC or FITC labeled dextran solution was applied. In the same study, if  $^{14}\text{C}$ -labelled poly(butyl cyanoacrylate) nanoparticles were placed into the chamber facing the brush border side of the porcine intestinal tissue in a two-chamber side-by-side diffusion cell, no radioactivity translocated to the acceptor chamber within 4 hours, if the mounted tissue came from the upper part of the small intestine. On the other hand, a significant amount of radioactivity was

observed in the acceptor chamber, when lower part of small intestine that possessed a considerable number of M-cells and Peyer's patches was mounted. Further evidence to prove the importance of Peyer's patches for the intestinal uptake of nanoparticles has been provided by Jani et. al. (26,29,37), who observed that uptake of nanoparticles into the Peyer's patches and passage *via* the mesentery lymph supply, leading to general circulation, in rats, increased with decrease in particle size. The surface properties of the nanoparticles may also have some influence on the uptake mechanism. Jani et. al. (29) observed that carboxylated polystyrene nanoparticles as compared to non-ionized polystyrene particles of similar particle size were taken up to a considerably lower degree.

It appears, therefore, that the major uptake pathway is via the M-cells and Peyer's patches in the gut attributed to the reduced amount of mucus. Additionally, particle size and surface properties of the nanoparticles play a crucial role in intestinal uptake of orally administered nanoparticles. However, it also suggests that major uptake pathway may be different in different regions of the small intestine (35).

As illustrated above, no uncertainty exists that absorbed nanoparticles appears in the blood stream. One such pathway of transportation is via lymphatic uptake and entry into the general circulation via the thoracic duct (Figure 1) (35). Another such pathway is the direct delivery of the nanoparticles from the intestinal wall into the blood capillaries, which involves crossing of two types of barrier upon their inter-epithelial or transcellular uptake (Figure 2) (28): the basement membrane (38,39) and the wall of the capillaries (35). Additionally,



occurrence of channels formed by fenestral diaphragms of variable sizes in the epithelial cells based on their location and surrounding physiological conditions (40), could permit nanoparticles to pass through the endothelium subsequently reaching to the capillaries (28).

In terms of kinetics, Volkheimer (31) reported an interesting observation: that the appearance of the particles in the blood does not represent a simple first-order process (absence of single blood level maximum). But rather, 2-3 maxima: first being very rapid (after few minutes), and a lag time of about 100 and 210 minutes between the second and third maxima respectively following oral administration. These multiple maxima thus indicate the possibility of different uptake mechanism as discussed earlier.

### **2.3. Brain targeting of surface modified nanoparticles**

As discussed in previous section, that the BBB represents an insurmountable barrier for the delivery of substantial number of drugs to the brain. One of the possibilities to tackle this challenge is by using surface modified nanoparticles for achieving drug delivery to the brain. Various drugs, such as loperamide, tubocurarine, doxorubicin, dipeptide kytorphin (41) and hexapeptide dalargin (6), were loaded on the surface modified nanoparticles and administered *via* either intravenous injections or peroral administration. Amongst these drugs, the most encouraging results were obtained with doxorubicin for the treatment of brain tumors. Intravenous injection of polysorbate80-coated nanoparticles loaded with doxorubicin (5 mg/kg) in rats achieved high brain levels of 6 µg/g of brain tissue as compared to controls (including the solution of polysorbate 80

containing doxorubicin along with uncoated nanoparticles) (41). The possible mechanism of the doxorubicin transport across the BBB has been postulated to be *via* endocytic uptake by the brain capillary endothelial cells followed either by release of the drugs in these cells and diffusion into the brain or by transcytosis. Additionally, the injected nanoparticles adsorb apolipoprotein E (apo E) or apo B in the systemic circulation to facilitate the interaction with the low-density lipoprotein receptor in the brain followed by endocytic uptake, representing the uptake of naturally occurring lipoproteins. This hypothesis was well supported by the achievement of antinociceptive effect using dalargin-loaded poly(butyl cyanoacrylate) nanoparticles with surface adsorbed apo E or loperamide-loaded albumin nanoparticles with apo E as a covalently attached homing device (41).

In one such study to demonstrate the uptake of dalargin loaded biodegradable poly(butyl cyanoacrylate) nanoparticles as a result of overcoating with surfactants such as polysorbate 80 and polyethylene glycol (PEG) 20000, Das and Lin (6) reported a significant dose- and time- dependent pharmacological effects in the CNS following oral administration into mice, whereas all controls, did not achieve dalargin-induced analgesia. The results clearly indicates that the drugs loaded on double-coated poly(butyl cyanoacrylate) indeed crossed the GI barrier and after oral administration and were transported across the BBB (6). Similar results were obtained by over coating of biodegradable nanoparticles when administered orally (11). Additionally, these nanoparticles also retained their targeting potential when coated with polysorbate 20, 40 and 60 contraries to this, large number of other surfactants were not able to achieve delivery across the

BBB (42). Give these *in vivo* observations demonstrating nanoparticle mediated drug uptake by the BBB, important questions need to be addressed. These includes: 1) mechanism of nanoparticle-mediated drug uptake by the BBB, 2) influence of surface properties in targeting efficiency, 3) quantification of drug at target site transported via this pathway to achieve significant pharmacological effects with reduced toxicity to the healthy cells (7)

Two major possibilities were reported by Kreuter. J (7) to elucidate the mechanism of nanoparticle-mediated uptake of drugs into the brain: 1) endocytosis by the endothelial cells with subsequent release of the drugs within these cells and delivery to brain, 2) transcytosis through the endothelial cell layer (43). This mechanism has been demonstrated by *in vitro* studies of nanoparticles over coated by polysorbate 80 into several primary endothelial cell lines including mice (44), rat (45) as well as primary bovine (46,47) and human endothelial cells (47). Additionally, *in vitro* studies also demonstrated the surface adsorption of apolipoproteins E or A-I (apo E or apo A-I) of nanoparticles coated with polysorbate 80 upon their incubation in blood plasma (48).

For this reason, *in vivo* experiments were performed (49), which concluded that polysorbate 80 specifically mimics as an anchor for the apolipoprotein which interact with low density lipoprotein (LDL) receptors on the brain capillary endothelial cells (50–52). This hypothesis was then challenged by Michaelis et. al. (53) and wherein pronounced antinociceptive effects was achieved when human serum albumin nanoparticles covalently bound to apo-E instead of cyanoacrylate nanoparticles with polysorbate 80 overcoat was used.

Later, comparable results were obtained by Kreuter et. al. (54) by covalently attaching apo A-I or apo B-100 to serum albumin nanoparticles. Apo A-I can interact with the scavenger receptor class B type I (SR-BI) (55,56) whereas, apo E and B with the LDL receptor. Therefore, interaction with these receptors, followed by endocytosis and transcytosis across the brain capillary endothelial cells appears to be the underlying mechanism for surfactant-coated nanoparticle mediated drug delivery, or albumin nanoparticles with adsorbed or covalently linked homing device such as the apolipoprotein A-I, B and E. The nanoparticle thus would mimic lipoprotein particles and act as trojan horses for LDL receptors (7).

#### **2.4. Fabrication of nanoparticles**

A major requirement for nanoparticulate mediated uptake of drugs to brain is the biodegradable property of nanoparticles. Non-biodegradable nanoparticles such as fullerenes, metal particles, and toxic systems such as quantum dots, or potential risky needle-shaped delivery system such as carbon nanotubes, might have hazardous effects like asbestos. Therefore, non-biodegradable nanoparticles might not be useful for drug delivery (57).

For this reason, three major types of biodegradable nanoparticulate materials like poly (alkyl cyanoacrylates) (PACAs) such as poly (butyl cyanoacrylate), poly(lactic acid) or its copolymer poly(lactide-co-glycolide) (PLGA), and human serum albumin have been the material of choice (57). Of these material, poly (butyl cyanoacrylate) has comparatively faster biodegradation, but it was not employed as polymers until the early 1980s (58).

However, the corresponding monomers, alkyl cyanoacrylates, have been used since 1966 for their excellent adhesive properties, resulting from the bonds of high strength they are able to form with most polar substrates, including living tissues and the skin (59). Therefore, these monomers have been extensively used as tissue adhesives for skin wound closure (60–62), as embolic material for endovascular surgery and as surgical glue (63). Many researches have also reported the successful use of PACA as nanoparticulate carriers (64–67). Moreover, the use of PACA as drug nanoparticulate carriers has gained increasing interest in therapeutics, especially in case for cancer treatments (68). Today, PACA nanoparticles are considered as one of the most promising polymeric nanoparticulate carrier system and are already in clinical development for its potential use in cancer therapy (12,69). They can be prepared by four major methods, such as emulsion polymerization, polymerization in a continuous aqueous phase, emulsion polymerization in a continuous organic phase, and interfacial polymerization (70,71). Among which, emulsion polymerization has been widely employed for fabrication of nanoparticles, and hence will be reviewed in detail, while others will be shortly reviewed.

Emulsion polymerization is amongst the most popular approach used to synthesize polymer colloids with matrix structure. The polymerization medium is generally aqueous making the process less hazardous. The cyanoacrylate monomers can be added in concentration between 0.05-7% (72). An anionic polymerization mechanism has been proposed, which is initiated by bases present in the aqueous polymerization medium. The cyanoacrylates are mainly initiated

by the hydroxy ( $\text{OH}^-$ ) ions either resulting from the dissociation of water or in some cases basic drugs. This hydroxyl ion induced polymerization is rapid and for this reason the pH of the aqueous medium is kept below 3.5 and with some drugs even below 1.0, to enable the formation of nanoparticles. Concomitantly, this polymerization generates hydrogen ( $\text{H}^+$ ) ions, wherein the hydrogen ion terminates the reaction. As a result of this termination, the molecular weights after the polymerization is very low and has been observed to be inversely related to change in pH (72,73). Due to low molecular weights, the nanoparticles are prone to agglomeration. And for this reason, stabilizers (e.g., high molecular weights dextran) are added to the system, which also significantly influences particle size and molecular weights (74,75). However, the influence of pH on particle size is somewhat different: particle size minimum exists around a pH of 2, whereas polydispersity falls with increasing pH, until a plateau is reached at pH 2.5 and above. Other factors contributing to the particle size of the nanoparticles includes monomer concentration and the stirring speed. Wherein a slight particle size minimum observed at monomer concentration of about 2% (74) and slight increase in particle size with increasing stirring speed.

Emulsion polymerization in a continuous organic phase was one of the first process employed to produce nanoparticles (76–78). PACA nanoparticles were obtained by adding the cyanoacrylate monomer to continuous organic phase due to its high solubility in organic solvent. Consequently, small percentage of nanoparticles with a shell-like wall (nanocapsules) along with solid, monolithic nanoparticles were obtained (79). The formation of PACA nanoparticles by

employing interfacial polymerization in an aqueous surrounding phase was introduced by Al Khouri Fallouh et.al. (80). Wherein the cyanoacrylate monomer as well as the oil-soluble drug were dissolved in a mixture of oil and ethanol in ratio of about 1:10 to 1:200. The organic solution containing the drug and the monomer was then added slowly through a tube or needle into water or buffer solution (pH 3-9) containing surfactant such as poloxamer 188 or 407 or phospholipids, which resulted in the spontaneous formation of nanocapsules consisting of an internal oil droplet surrounded by polymeric wall (81).

## **2.5. Fabrication of oral double-coated nanoparticles for brain delivery**

In designing of oral drug delivery systems, the stability of the loaded drug within the polymeric carrier matrix upon its contact with GI fluids plays a crucial role. This consideration is especially important, if the loaded drugs is acid-labile and if the polymeric carrier is biodegradable. One of the proposed strategies for protecting biodegradable polymers and the entrapped labile drug from the effects of the GI fluids can be obtained by application of polymeric coating such as poly(ethylene) glycol (PEG) and the process referred as PEGylation (82–85).

In the event of any ‘foreign’ particulate reaching the circulation following oral absorption, there lies an obvious problem of clearance by the reticulo-endocytic system (RES). So, for any nanoparticle increase of circulation half-life is an essential for it to stay in the blood for an extended period while retaining its targeting potential. Such a long circulating effect can be achieved by employing ‘stealth’ or sterically stabilized properties by PEG coat over nanoparticles (86,87). Generally, the assumed mechanism is the formation of, hydrophilic

coating, to avoid opsonization by the plasma proteins and due to the dynamic structure of PEG, the immune system experiences difficulties in modelling an antibody around it (88). It is generally agreed, that only if a polymer chain possesses both hydrophilicity and flexibility properties (to enable a high number of possible chain conformations) can serve as an effective protecting coat for particles against opsonization (89). Additionally, it has been proposed that both reduction of adsorption of opsonin and selective adsorption of certain components of plasma (dyopsosins) prevent the recognition as well as uptake of nanoparticles by the macrophages. Researches on the usage of PEG over coat for 'stealth' properties, now agree that PEG is termed as a 'dysphonic' polymer which by virtue of its selectivity in adsorption of two serum components (one with molecular weight below 30,000 Dalton (Da) and the other with a molecular weight higher than 100,000 Da) leads in a dysphonic action (90).

Thus, for nanoparticles that could survive oral administration and still retain targeting properties to brain, a 'double coat' of PEG and polysorbate 80 can be hypothesized. PEG as discussed above is well known for its protective action in the GI environment along with its ability to enhance the circulation half-life of nanoparticles. On the other hand, requirement of polysorbate 80 coating for apo E mediated brain targeting of nanoparticles has been discussed in earlier sections. In addition to the use of PEG to impart stealth properties, polysorbate 80 over coat might also be useful in GI uptake of particulate by fluidizing action on the mucus barrier, one of the factors that can be exploited in attempts to improve GI uptake of the particulates (91,92).



If nanoparticles are coated with an appropriate surfactant, then the extent of particulate aggregation or entrapment in mucus can be reduced and uptake can be enhanced (93). Therefore, in order to facilitate the uptake of nanoparticles by the GI tract and subsequent delivery to brain via oral route, a ‘double-coating’ of polymeric nanoparticles with high molecular weight PEG and polysorbate 80 has been hypothesized. However, its success would depend on the stability of such double coat in the biological systems. It is also to be appreciated that the choice of PEG and polysorbate 80 as coating agents is dictated by number of physiological factors, which can impart targeting and protective properties to nanoparticles.

## **2.6. Characterization of nanoparticles**

### **2.6.1. Physicochemical characterization**

Several physicochemical methods (Table 1) exists for the characterization of nanoparticles. Among which particle size plays a crucial role and is most eminent feature of nanoparticles. However, other parameters, such as density, molecular weight, and crystallinity, largely influences the drug release and degradation. Whereas surface properties, such as the surface charge, hydrophilicity and hydrophobicity, significantly influence the interaction of these particles with the biological environment and the resulting bio-distribution.

One of the fastest and routinely applied method for size measurements are dynamic light scattering or photon correlation spectroscopy (94). Photon correlation spectroscopy determines the hydrodynamic diameter of the nanoparticles via Brownian motion. Therefore, the particle size analysis measurements are influenced by the interaction of these particles with the

surrounding medium. Consequently, the exact viscosity of the medium should be known. Another method of size determination employs microscopic evaluation and scanning electron microscopes (SEM) as well as transmission electron microscope (TEM) are frequently used for this purpose. In addition to size determination, SEM and TEM are used for analysis of morphological properties of the particles (for example: porosity of the particles).

The molecular weights of polymeric nanoparticles are mainly determined by dissolution of the particles in a suitable solvent followed by gel permeation chromatography. However, this method is limited in its applicability due to the lack of availability of polymer standards required to validate the results obtained (95–97), (72).

Information about crystalline structure of nanoparticle may be obtained by x-ray diffraction (94), differential scanning calorimetry (DSC), differential thermal analysis (DTA), thermal gravimetric analysis (TGA), thermal mechanical analysis (TMA) and thermal optical analysis (TOA) (98,99). These methods can be quite useful in cases where small drug molecules are entrapped in the polymer network in the form of an amorphous solid solution (100).

Hydrophobicity of the nanoparticles surface seems to have a much larger influence on bio-distribution after intravenous injection. Water contact angle measurements (101) and hydrophobic interaction chromatography (102) are two major methods for the determination of hydrophobicity, since contact angle measurements can be performed on the flat surfaces, and not on hydrated nanoparticles in their dispersion media. As a result, hydrophobic interaction

chromatography seems to be an efficient, although labor intensive method (102,103).

### **2.6.2. Degradation pathway of polymeric nanoparticles**

PACA are biodegradable polymers for which complete excretion of the polymer material will occur if the nanoparticles were designed using low-molecular weight polymers. The degradation of poly(alkyl cyanoacrylate) is studied extensively, and two major degradation pathways has been described in the literature. Firstly, degradation of polymer by erosion of the polymeric backbone under formation of formaldehyde (104–106). Secondly, lysis of the ester bond leading to the formation of soluble polymer acid *in vivo* (107).

Degradation product by this pathway results in the formation of an alkyl alcohol and poly(cyanoacrylic acid), which are soluble in water and readily eliminated via kidney filtration. This degradation has been shown to be catalyzed by esterases from serum, lysosomes and pancreatic juice (108). According to this mechanism, nanoparticles are usually degraded within a couple of hours depending on the alkyl side chain length of the PACA forming the nanoparticles (109).

### **2.6.3. Drug release**

Nanoparticle exhibit their special drug delivery effects (110) in most cases by direct interaction with biological environment. Subsequently, the drug release may occur by desorption of surface-bound drug, diffusion through polymeric matrix, nanoparticle matrix erosion, or a combined erosion and diffusion processes.

The release mechanism (matrix- type device), diffusion coefficient, biodegradation rate of the polymeric backbone are the three main factors controlling the drug release rate from the polymeric nanoparticles (111). Additionally, release of the drug is also greatly influenced by the biological environment, which is more pronounced as compared to conventional dosage forms (e.g., tablets and capsules) as nanoparticles may be coated by plasma proteins resulting in imparting an additional diffusional barrier leading to a retardation in drug release. In addition, nanoparticles may have enhanced interaction with biological or artificial membrane, leading to enhanced delivery of drugs through these membranes in comparison to a simple solution (110).

An important point to consider is the quantification of the drug release from these nanoparticles is technically difficult to achieve. This can be attributed to the inability of the rapid and effective separation of the nanoparticle from the dissolved or released drug in the surrounding medium owing to very small size of the dosage form. At least five different methods for determination of *in vitro* drug release, such as side-by-side diffusion cells with artificial or biological membrane (110,112), dialysis bag diffusion (79,113,114), reverse dialysis sac (115), ultracentrifugation (by analyzing the supernatant at pre-determined time points) (116,117), ultrafiltration (79) have been reported.

### **3. Research objectives and specific aims**

There are three principle objectives of this research study. The first objective is to fabricate double-coated doxorubicin-loaded poly(butyl cyanoacrylate) nanoparticles of less than 300 nm to facilitate lymphatic uptake and thereby by-pass the first-pass metabolism. The second major objective is to evaluate their brain targeting potential after oral administration in rats. The third major objective is to evaluate the potential of these double-coated doxorubicin loaded nanoparticles in reversing the multidrug resistance

#### **Specific aims include:**

1. To fabricate double-coated doxorubicin-loaded biodegradable polymeric nanoparticles composed of poly(butyl cyanoacrylate) with double-coats with Tween 80 and PEG 20000 at various concentration level.
2. To characterize the fabricated nanoparticles based on their particle size, zeta-potential, entrapment efficiency, drug leakage in various simulated mediums (i.e., intestinal fluid and serum).
3. To evaluate the brain distribution of double-coated doxorubicin loaded poly(butyl cyanoacrylate) nanoparticles after oral administration in Sprague Dawley rats and based on pharmacokinetic study evaluate the role of lymphatics in the oral absorption of double-coated doxorubicin loaded poly(butyl cyanoacrylate) nanoparticles.
4. To investigate the potential of the fabricated double-coated doxorubicin nanoparticles in the reversal of multi-drug resistance by cell uptake study or

MTT assays using cell lines characterized for overexpression of P-gp and BCRP transporters.

#### **4. Materials and methods**

##### **4.1. Materials**

The monomer n-2-butyl cyanoacrylate was purchased from Glustitch Inc (Delta, Canada). Doxorubicin hydrochloride (henceforth referred as doxorubicin) was purchased from BOCSCI Inc. (Shirley, New York). Dextran 70, sodium chloride, pepsin, monobasic potassium phosphate, pancreatin, sodium taurocholate, polyethylene glycol (PEG) 20000, 1% penicillin/streptomycin solution, Whatman® microfiber pre-filters (2.5, 0.6 and 0.3 µm), TritonX-100, sucrose, sodium azide, dynasore, and ammonium chloride were purchased from VWR International (Radnor, PA). 1X Dulbecco's phosphate buffered saline (DPBS) and bovine serum (henceforth referred as serum) were purchased from HyClone™ (Logan, UT). Super Refined™ polysorbate 80 (Tween 80) was a generous gift from Croda (Edison, NJ). The mouse brain endothelial (bEnd.3) cells, 0.25% trypsin, and Dulbecco's modified eagle medium (DMEM) (30-2002) were obtained from American Type Culture Collection (Manassas, VA). The human colon cancer cell line SW620 and its doxorubicin-selected P-gp-overexpressing SW620/Ad300 cells (henceforth referred to as AD300), the NSCLC cell line NCI-H460 and its mitoxantrone-selected BCRP-overexpressing NCI-H460/MX20 cells (henceforth referred to as AD300), were used for P-gp and BCRP reversal study, respectively. Fetal bovine serum (non-heat activated) was obtained from Atlanta Biologicals (Flowery Branch, GA). All reagents were of

analytical grade and were used as received. Finally, previously published literatures were used for preparation of release medium (pH 4.8) (118), and fasted state simulated intestinal fluid (FaSSIF) (119).

## **4.2. Analysis of doxorubicin**

### **4.2.1. UV-Vis spectroscopy method**

The doxorubicin content in samples obtained from in vitro performance studies was determined using UV-Vis Spectrophotometer (DU 700 series, Beckman Coulter Inc., Brea, CA). At a preset wavelength of 480 nm, a peak, characteristic of doxorubicin, has been reported (120). Serial dilutions of stock doxorubicin solution (1000 µg/ml) were made to obtain concentrations ranging from 0.1 to 50 µg/ml. Linear regression analysis was performed between the absorbance and the concentration of doxorubicin to establish the calibration curve using SigmaPlot 12.5 (Systat Software Inc., San Jose, CA).

### **4.2.2. Fluorescence spectroscopy method (plate-reader method)**

The doxorubicin content from in vitro cell culture and in vivo studies was determined using SpectraMax M5<sup>e</sup> (Molecular Devices, Sunnyvale, CA) at  $\lambda_{\text{ex}}=480$  nm,  $\lambda_{\text{em}}=560$  nm (121). For in vitro cell culture studies, serial dilutions of stock doxorubicin solution were made to obtain various concentrations (0.033 to 3.33 µg/ml). Linear regression analysis was performed to establish the calibration curve using SigmaPlot 12.5.

For in vivo samples, rat serum and tissue homogenates were spiked with standard doxorubicin solution to obtain final concentrations (0.001 to 200 µg/ml). Serum samples were then processed as described in the literature (122). Tissue

homogenates were subjected to an additional lysis step by 1% TritonX-100. The lysates were then extracted for determination of doxorubicin like serum samples. Serum and tissue homogenates samples were analyzed by fluorescence spectroscopy method and data was processed as described above.

#### **4.2.3. Fluorescent microscopy method**

The intracellular accumulation of doxorubicin was studied by using fluorescence microscopy reported in the literature (123). SW620 cells were chosen for their ability to take up doxorubicin readily. The images of the SW620 cells after treatment (i.e., incubation with doxorubicin in solution for a predetermined period) along with the control (i.e., untreated cells) were collected using EVOS® FL Auto Imaging System (Model AMFAD1000) (Thermo Fisher Scientific, Fair Lawn, NJ). In order to take the images, the cells were visualized at a total magnification of 1200× (40× objective with an internal magnification of 30×) using two different modes (i.e., phase contrast and fluorescence). Phase contrast was used to locate a region of cells free from any cellular debris and/or any overlapping cells. Fluorescence was used to determine doxorubicin accumulation within the cells, which was achieved by selecting the RFP filter (built-in the instrument) at a preset wavelength (excitation: 552 nm; emission: 585 nm). For both phase contrast as well as fluorescence, images of cells were acquired using a monochrome camera also built-in the instrument.



### **4.3. Fabrication of double-coated doxorubicin-loaded poly(butyl cyanoacrylate) nanoparticles delivery systems (PBCA-NPDS)**

The fabrication process of these formulations is illustrated in Figure 3 representing core (Figure 3A), and single- (Figure 3B) and double-coated formulations (Figure 3C).

#### **4.3.1. Doxorubicin-loaded PBCA-NPDS**

The doxorubicin-loaded PBCA-NPDS were prepared by an anionic polymerization method as reported, with modifications (124). Briefly, dextran 70 (1.5% w/w) was added to 0.001 N HCl solution in Nanopure® water (pH 3.00) under constant magnetic stirring at low speed (500-800 rpm) with a Pyrex® Spinbar® (VWR International, Radnor, PA). Once dextran 70 was completely solubilized, butyl cyanoacrylate monomer solution (1% v/v) was added dropwise. After 40 minutes of polymerization, doxorubicin (0.4% w/v) was then added. Following 4 hours of polymerization, the dark red nanoparticle suspension was neutralized with sodium hydroxide (0.1 N) and further stirred for an additional 12 hours to ensure complete neutralization. The nanoparticle suspension obtained was then subjected to sequential filtration step using 1.2 µm, and 0.7 µm filters with a vacuum filtration assembly. The filtered suspension was further subjected to ultracentrifugation for two cycles (10 minutes each at 40000 rpm and 4-6°C) using Optima XE ultracentrifuge, rotor Type 70 Ti (Beckman Coulter, Indianapolis, IN). After each centrifugation step, the supernatant was removed, and the nanoparticles were resuspended in the same amount of Nanopure® water using brief sonication. Finally, the pelleted nanoparticles were immediately frozen

using a freezing mixture of dry ice and alcohol. The frozen nanoparticles were then immediately lyophilized using a Freezone 4.5 lyophilizer (Labconco, Kansas City, MO). Lyophilization was carried out at  $-51^{\circ}\text{C}$  and at a pressure of 0.018 mbar in the presence of 4% trehalose as a cryoprotectant overnight and then stored at  $2-8^{\circ}\text{C}$  until further use.

When adding the doxorubicin during the polymerization, there remains an obvious challenge of any undesirable chemical interaction between the doxorubicin and nanoparticle backbone. This challenge intensifies, if the drug has a reactive functional group (i.e., amine in doxorubicin). And, the polymer (poly butyl cyanoacrylate group) has an ester group. Ester may covalently react with amine to form amides. However, such reaction require microwave irradiation (125), activated acid derivatives (126), or a catalyst (127). Since none of these procedures were used in this study, no interaction between doxorubicin and the monomer (butyl cyanoacrylate) has been hypothesized. To test this hypothesis, the lyophilized doxorubicin-loaded PBCA-NPDS were analyzed by  $^1\text{H}$  nuclear magnetic resonance (NMR) spectroscopy. This method is routinely used for structural characterization and verification of chemical compounds based on the bonding characteristics of the hydrogen atom. Briefly, samples were obtained by dissolving the doxorubicin-loaded nanoparticles and free doxorubicin (control), respectively, in deuterated-dimethyl sulfoxide ( $\text{DMSO-d}_6$ ). The solutions were then filled in NMR tubes and were analyzed using NMR instrument (Bruker, Billerica, MA). Samples were locked using an auto-shim mode, and spectrum

acquisition was performed using TopSpin mode and number of scans were fixed to 16 (default settings).

It should be noted that these doxorubicin-loaded PBCA-NPDS were sequentially coated with either Tween 80 or PEG 20000 (single-coated) and with Tween 80 and PEG 20000 (double-coated) as described below.

#### **4.3.2. Single-coating of doxorubicin-loaded PBCA-NPDS**

About half of the doxorubicin-loaded PBCA-NPDS obtained from the above step were coated with varying concentrations of up to 2% of Tween 80 relative to the total suspension of nanoparticles in DPBS. Depending upon the amount of coating of Tween 80 used for formulation, T1 (1% Tween 80) or T2 (2% Tween 80) was assigned as part of the formulation code. For each formulation, the required quantities of Tween 80 were added to the above suspension. This suspension was then kept in a water-shaker bath, maintained at  $25^{\circ} \pm 0.5^{\circ} \text{C}$  and 100-120 cycles per minute for 90 minutes.

About a quarter of doxorubicin-loaded PBCA-NPDS obtained were coated with 1% of PEG 20000 in the same way as described above. Since these formulations did not contain Tween 80, they were categorized under single-coated formulation.

#### **4.3.3. Double-coating of doxorubicin-loaded PBCA-NPDS**

About half of Tween 80 overcoated doxorubicin-loaded PBCA-NPDS obtained from the above step was further overcoated with varying concentrations of up to 2% of PEG 20000 relative to the total suspension of nanoparticles in DPBS. Depending upon the amount of coating of PEG 20000 used for

formulation, P1 (1% PEG 20000) or P2 (2% PEG 20000) was assigned as part of the formulation code. For each formulation, the required quantities of PEG 20000 was added to the above suspension. This suspension was then kept in a water-shaker bath, maintained at  $25^{\circ} \pm 0.5^{\circ}$  C and 100-120 cycles per minute for 90 minutes. Thereafter, the suspension of these double-coated doxorubicin-loaded PBCA-NPDS was further stirred for overnight to ensure complete equilibration of coating material (Tween 80 and PEG 20000) with doxorubicin-loaded PBCA-NPDS.

#### **4.4. In vitro evaluation of double-coated doxorubicin-loaded PBCA-NPDS**

All doxorubicin-loaded PBCA-NPDS (core, single- and double-coated) formulations were evaluated and characterized by their particle size, zeta potential, entrapment efficiency, drug release and drug leakage.

##### **4.4.1. Particle size and zeta potential**

All formulations (5 mg) were suspended in 1 ml DPBS by brief sonication. This homogenous suspension was then transferred to a folded capillary cell (DTS1070) (Malvern Panalytical Inc. Westborough, MA). After a brief equilibration period inside the sample chamber, the mean hydrodynamic particle size (nm), the polydispersity of size distribution (PDI) and zeta potential were measured. For particle size analysis, dynamic light scattering along with Non-Invasive Back Scatter Technology built-in the Zetasizer Nano ZS (Malvern Panalytical Inc. Westborough, MA) was used. Zeta potential was measured using laser doppler micro-electrophoresis also built-in the Zetasizer Nano ZS.

#### 4.4.2. Entrapment efficiency

The amount of drug entrapped was determined by completely dissolving the lyophilized doxorubicin-loaded PBCA-NPDS (5.50 mg) in 5 ml methanol:acetonitrile (50:50) solution. The resulting solution was centrifuged at 13300 rpm for 10 minutes at  $4^{\circ} \pm 0.5^{\circ}\text{C}$  to pelletize any undissolved materials. The clear supernatant was analyzed for doxorubicin content by the UV-Vis spectroscopy method described previously. The entrapment efficiency of doxorubicin was then calculated as a ratio of the assayed doxorubicin in lyophilized doxorubicin-loaded PBCA-NPDS to the total doxorubicin (i.e., 400 mg) used in the fabrication as reported in the literature and shown below (128)

$$\text{Entrapment efficiency (\%)} = \frac{\text{Weight of drug in nanoparticles}}{\text{Weight of drug fed initially}} \times 100 \quad \text{Equation 1}$$

#### 4.4.3. In vitro drug release kinetics

Among various methods to study the drug release from various nano-formulations (liposomes, nanoparticles, etc.), usage of the dialysis membrane bag has been widely discussed in literatures (129–134). However, the selection criteria of a dialysis membrane bag over another is seldom reported (134,135). Therefore, the evaluation of various types of dialysis membrane bags and the effect of doxorubicin concentration on its diffusion rate through dialysis membrane bags were performed, prior to *in vitro* drug release study.

##### 4.4.3.1. Screening of dialysis membrane bags

The selective diffusion of drugs (based on molecular weight) across a semi-permeable dialysis membrane bags is the main principle to separate the drug released from nano-formulations and subsequently allow the sampling of drug

released. Four different Float-A-Lyzer G2 dialysis membrane bags (Repligen, Waltham, MA) of different MWCOs (i.e., 50, 100, 300, and 1000 KDa) were evaluated. Briefly, doxorubicin standard solution (1 mg/ml) was prepared by dissolving the desired amount of doxorubicin in the release medium and 1 ml of this standard solution was transferred to inside each of the hydrated dialysis membrane bags as per the user's manual provided by the manufacturer. These sealed dialysis membrane bags were then placed into 50 ml polypropylene tubes having 20 ml release medium at  $37^{\circ} \pm 0.5^{\circ}\text{C}$  and 100-120 rpm using a water-shaker bath. At pre-determined time intervals (i.e., 1, 2, 3, 4, 5, and 6 hours), aliquots (1 ml each) were withdrawn from the outside of the dialysis membrane bags and replaced by an equal volume of release medium. The aliquots were analyzed for doxorubicin content using the UV-Vis spectroscopy method described previously.

#### **4.4.3.2. In vitro release study**

All lyophilized doxorubicin-loaded PBCA-NPDS formulations (equivalent to 5.60 mg of doxorubicin) were suspended in 5 ml of release medium, respectively. The resulting nanoparticle suspension were transferred to inside of the hydrated dialysis membrane bags. After seating the bags, they were then placed into flat bottom glass tubes (130 mm  $\times$  40 mm) having 100 ml release medium at  $37^{\circ} \pm 0.5^{\circ}\text{C}$  and 100-120 rpm. At pre-determined time intervals (i.e., 1, 2, 3, 6, 9, 12, 24, 36, 48, 60, and 72 hours), aliquots (1 ml each) were withdrawn from the receiver and replaced by an equal volume of release medium.

The released doxorubicin in aliquots was determined by the UV-Vis spectroscopy method described previously.

#### **4.4.4. Drug-leakage in various simulated mediums**

To maximize the payload of doxorubicin at the target site following oral administration, drug leakage from dosage forms in the gastrointestinal tract and serum was evaluated.

##### **4.4.4.1. Fasted state simulated intestinal fluids (FaSSIF)**

Lyophilized doxorubicin-loaded PBCA-NPDS formulations (5.60 mg) were dispersed in 1 ml FaSSIF. The dispersions were then transferred into dialysis membrane bags (MWCOs: 1000 KDa) and dialysis was performed in tubes containing 30 ml FaSSIF at 37°C 100-120 rpm for 12 hours. Thereafter, an aliquot was withdrawn from the receiver and analyzed for doxorubicin content by the UV-Vis spectroscopy method described previously.

##### **4.4.4.2. Serum**

The leakage study in serum was performed by dispersing lyophilized doxorubicin-loaded PBCA-NPDS formulations (5 mg) in 10 ml of serum at 37°C and 100-120 rpm for 3 hours. After this time, aliquots were subjected to protein precipitation and drug extraction using ice-cold methanol. The extracts were analyzed for doxorubicin content by the UV-Vis spectroscopy method described previously.

## **4.5. In vitro model to elucidate the brain uptake mechanism**

### **4.5.1. Uptake mechanism elucidation using specific inhibitors as a pretreatment**

For uptake mechanism elucidation, we hypothesize that pretreating the bEnd.3 cells with inhibitors of transporters responsible for up taking nanoparticles would impact the uptake of doxorubicin within the same cells upon further incubation with formulation T2P2 or free doxorubicin in solution (control). Based on this hypothesis, bEnd.3 cells were pretreated with the growth media (no pretreatment) as a control group. In addition, cells were pretreated with an endocytosis inhibitor sodium azide (0.1%w/v) (136), and by incubation at 4°C. To evaluate the role of clathrin-mediated endocytosis, cells were pretreated with sucrose (0.45 M) (137). Since bEnd.3 cells also expresses LDL receptors (138), cells were pretreated with LDL receptor inhibitor dynasore (5 µM) (139). Furthermore, to evaluate the involvement of the endosomal/lysosomal compartments in the trafficking of nanoparticles pretreatment with lysosomotropic agent ammonium chloride (140) was performed. After initial pretreatment (i.e., 1 hours), the cells were washed with cold DPBS. Thereafter, pretreated cells were further incubated with formulation T2P2 or free doxorubicin in solution (control) for additional 3 hours, followed by cell lysis by mixture of 0.1 ml of equimolar mixture of 1% TritonX-100 and 0.2 N sodium hydroxide, and 0.4 ml of methanol and doxorubicin content determination by the fluorescence spectroscopy method described previously. Furthermore, any potential



cytotoxicity of inhibitors on bEnd.3 cells was investigated by modified MTT colorimetric assay (141), by incubating the cells for 4 hours with various inhibitors at concentration levels described above.

#### 4.5.2. Permeability screening study

Permeability screening study was performed on bEnd.3 cells monolayer by seeding  $4 \times 10^5$  cells per Transwell® permeable support inserts (pore diameter: 0.4  $\mu\text{m}$ ). The integrity of the cell monolayer was checked at the beginning and the end of experiments by measuring the transepithelial electrical resistance (TEER) using EVOM2 (World Precision Instrument, Sarasota, FL). Additionally, leakage of Lucifer yellow (paracellular marker) across the monolayer was determined at the end of experiment. Permeability study were conducted by incubating formulation T2P2 or free doxorubicin solution (control) on the apical or basolateral side, at 37°C and 5% CO<sub>2</sub> for 2 hours. After this, the concentration of doxorubicin in the receptor compartment (i.e., basolateral or apical) was quantified by fluorescence spectrophotometric method described previously, and the apparent permeability coefficients ( $P_{app}$ ) were calculated as shown in Equation 2 (142).

$$P_{app} (cm.s^{-1}) = \frac{Q}{A \times C \times t} \quad \text{Equation 2}$$

Where,  $Q$  represents the total amount of permeated doxorubicin ( $\mu\text{g}$ ),  $A$  is the surface area of the filter ( $\text{cm}^2$ ),  $C$  is the initial doxorubicin concentration in the donor compartment ( $\mu\text{g.ml}^{-1}$ ), and  $t$  is the incubation time (s). For all permeability experiments, bEnd.3 cells were used prior to passage 35 (143).

#### **4.6. In vivo performance of double-coated doxorubicin loaded PBCA-NPDS**

The in vivo performance studies were evaluated using Sprague-Dawley (SD) rats (225-250 g) (Taconic Biosciences, Germantown, NY). All experiments were conducted as per approved protocol by Institutional Animal Care and Use Committee. Rats were divided into 4 groups with 4 rats in each group. Groups 1, 2, and 3 received formulation T2P2 at a dose equivalent to 27, 50, and 70 mg/kg of doxorubicin, respectively. Group 4 received free doxorubicin in solution at a dose of 70 mg/kg (control group). Two (2) routes of administration [i.e., intravenous- group 1, oral- group 2-4] were evaluated.

##### **4.6.1. Biodistribution study**

For biodistribution study, two (2) rats from each group (described above) were euthanized at 1 and 2 hours for group 1, and, 1 and 3 hours for groups 2-4 by carbon dioxide asphyxiation, and brain, and liver tissues were collected. Isolated tissues were immediately wiped to remove blood, subsequently, they were weighed and placed on ice immediately. For analysis, tissues were homogenized at 5000 rpm using VirTis TEMPEST I.Q<sup>2</sup> homogenizer (Tempest Inc., Cleveland, OH) and doxorubicin was extracted and determined as described previously.

##### **4.6.2. Pharmacokinetic study**

Following the dose administration (i.e., intravenous via the saphenous vein and oral gavage), blood samples were collected via tail clipping at predetermined time intervals for up to 2 hours and 3 hours for group-1 and group 2-4, respectively. Blood samples were collected in serum separating tubes

(MiniCollect® Tube) (Greiner Bio-One, Kremsmünster, Austria). Serum was separated, and doxorubicin concentration was determined as described previously.

#### **4.7. In vitro cell culture studies**

##### **4.7.1. Intracellular accumulation study of various in doxorubicin-loaded PBCA-NPDS in SW620, AD300 and bEnd.3 cell lines**

SW620 and AD300 were seeded in their respective growth medium in 24-well plate and cells were allowed to grow overnight at 37°C, 5% CO<sub>2</sub>. On the day of the experiment, cells were washed with DPBS (pH 7.4) three times.

Subsequently, the cells were treated with 5 µM free doxorubicin in solution, all nanoparticles formulations (equivalent to 5 µM doxorubicin), and blank (growth mediums). The treated cells were then incubated for 2 hours at 37°C, 5% CO<sub>2</sub>.

Following the incubation period, the treatment (free drug, nanoparticles formulations, or growth medium) was aspirated. The cells were then gently washed with DPBS three times. And, then immediately examined the cells using the fluorescence microscopy method described previously. For this study, single-coated formulations, free doxorubicin, and growth medium served as controls.

Since it is difficult to estimate the amount of up taken doxorubicin from microscopic images. An empirical parameter [i.e., corrected total cell fluorescence (CTCF)], expressed as fluorescence intensity, was chosen for indirect quantification of doxorubicin within the cell (144). CTCF was obtained after subtracting the intensity of the blank cells (background), from cells exhibiting fluorescence. This was performed using ImageJ® software (National

Institutes of Health, Bethesda, MD). Higher fluorescence intensity was used as a surrogate for higher intracellular accumulation of doxorubicin.

#### **4.7.2. Cytotoxicity determination of various doxorubicin-loaded PBCA-NPDS to evaluate their P-gp and BCRP efflux transporter inhibition potential**

The modified paraformaldehyde, 3-(4,5-dimethylthiazol-2-yl)-2,5-diphenyl-tetrazolium bromide (MTT) colorimetric assay was used to detect the sensitivity of cells to doxorubicin as well as double-coated doxorubicin-loaded PBCA-NPDS in vitro (141). Briefly, cells were loaded in 180  $\mu$ l of complete growth medium in 96-well plates in triplicate at cell density of 5000-6000 cells/well. After incubation at 37°C, 5% CO<sub>2</sub> for 24 h, cells were treated with different concentrations of free doxorubicin or double-coated doxorubicin-loaded PBCA-NPDS (20  $\mu$ l/well). After 72 h incubation at 37°C, 5% CO<sub>2</sub>, 20  $\mu$ l of MTT solution (4 mg/ml) was added to each well. The plates were further incubated at 37°C, 5% CO<sub>2</sub> for 4 h, enabling viable cells to change the yellow-colored MTT into dark-blue formazan crystals. Subsequently, the MTT/medium was carefully aspirated from each well without disturbing the cell, and 100  $\mu$ l of DMSO was added into each well. Plates were placed on shaking table to ensure thorough mixing of formazan into DMSO. Finally, the absorbance was determined at 570 nm using microplate reader (ThermoFisher Scientific, Waltham, MA) and data acquisition was performed by SkanIt™ software (ThermoFisher Scientific).

#### **4.8. Data analysis**

##### **4.8.1. Pharmacokinetic data analysis**

To overcome the limitation of sparse data in animal studies, pooled analysis of serum doxorubicin concentration-time curves obtained were analyzed using compartmental analysis using WinNonlin® (Pharsight, Cary, NC). The parameter estimation during the model fitting analysis was performed using a Gauss-Newton algorithm with Levenberg-Hartley modification. The Akaike information criteria (AIC), lack of systemic deviations in the residuals was considered as goodness of fit criteria (145). Equation 3 and 4 was employed for simultaneous model fitting of serum concentration-time profiles obtained after intravenous and oral administration, respectively.

$$C_p = Ae^{-\alpha t} + Be^{-\beta t} \quad \text{Equation 3}$$

where,  $C_p$  is the plasma concentration of doxorubicin at time  $t$ ,  $A$  is y-intercept of first-order rate process of distributive phase and  $B$  is y-intercept of first order process of elimination phase,  $\alpha$  is hybrid rate constant for distributive phase and  $\beta$  is hybrid rate constant for elimination phase.

$$C_p = Ae^{-\alpha(t-t_{lag})} + Be^{-\beta(t-t_{lag})} + Ce^{-ka(t-t_{lag})} \quad \text{Equation 4}$$

Where,  $A$  is y-intercept of first-order rate process of the absorption phase and  $B$  is y-intercept of first order process of distributive phase  $C$  is y-intercept of first-order process of elimination phase,  $ka$  is first-order absorption rate constant, and  $t_{lag}$  is the lag time associated with drug absorption. After obtaining the values of primary parameters (i.e.,  $A$ ,  $\alpha$ ,  $B$ , and  $\beta$ ) from model fitting analysis (Equation 3), the values of secondary parameters such as volume of distribution ( $V$ ), clearance ( $CL$ ) were further calculated using the WinNonlin. Thereafter, the drug and animal related parameters [i.e.,  $V$ , and  $CL$ ] were treated as fixed parameter during

the simultaneous model fitting analysis. This assumed that clearance remains constant between two study occasions (i.e., intravenous, and oral administration). Thereafter, the dosage form related parameters (i.e.,  $k_a$ , and  $t_{lag}$ ) were estimated by model fitting.

#### **4.8.2. Statistical analysis**

All the acquired data were expressed as mean  $\pm$  standard deviation (SD), and analyzed with SigmaStat 3.5 (Systat Software Inc., San Jose, CA).

Differences between multiple groups were evaluated by one-way analysis of variance (ANOVA) followed by Holm-Sidak post-hoc analysis to determine the groups, which showed significant difference. Differences between two groups were evaluated by the student's t-test. In each case, a  $p$ -value less than 0.05 was considered as a representation of significant difference.

### **5. Results and discussion**

#### **5.1. Analytical methodology**

The absorbance (Figure 4) and fluorescence intensity (Figure 5) were found to increase linearly with the concentration of doxorubicin within the measured concentration range with a regression coefficient ( $r^2$ ) value of more than 0.995. These results indicated that both the UV-Vis and fluorescence spectroscopy method, adopted for the detection and quantification of doxorubicin, are reliable methods. Furthermore, an ease of visualization of the drug by fluorescent microscopy method (Figure 6) also indicates its suitability for its usage in determination of doxorubicin.

## **5.2. Fabrication and characterization of double-coated doxorubicin loaded PBCA-NPDS**

For convenience in terminology, all formulations were coded based on the level of Tween 80 and PEG 20000 coating. For example, formulation T2P2 (representing 2% Tween 80 and 2% PEG 20000). The particle size, polydispersity index (PDI), zeta potential and entrapment efficiency of various non-coated and coated doxorubicin-loaded PBCA-NPDS formulations in comparison with blank PBCA-NPDS nanoparticles (placebo) are summarized in Table 2. And, <sup>1</sup>H NMR spectrum to evaluate the interaction of the polymeric core with doxorubicin is shown in Figure 7.

As expected, the mean particle size of doxorubicin-loaded PBCA-NPDS (formulation T0P0) increased due to doxorubicin loading as compared to that of blank PBCA-NPDS (154.5 nm vs. 109.4 nm). This increase in size could be attributed to interference in the surface deposition of dextran 70 (surfactant) chains caused by the presence of the doxorubicin during the polymerization step. As a result, their adsorption on PBCA-NPDS may have reduced, leading to an increase in the particle size (146). Further coating of doxorubicin-loaded PBCA-NPDS with Tween 80 and PEG 20000 at 1%, respectively, the mean particle size of single-coated doxorubicin-loaded PBCA-NPDS increased to 182.6 nm (formulation T0P1) or remained similar size at 154.4 nm (formulation T1P0). This could be attributed to the high MW of PEGs (MW > 5000 Da) resulted in the formation of a layer-wise polymeric network on the surface of PBCA-NPDS (147). Furthermore, with a double coating with Tween 80 at 1% and PEG 20000

at either 1% or 2%, mean particle size of the double-coated formulations increased from 154.4 nm (formulation T1P0) to 203.6 nm (formulation T1P1) and 256.9 nm (formulation T1P2). In addition, with double coating with Tween 80 at either 1% or 2% and PEG 20000 at 1%, mean particle size of the double-coated formulations increased from 182.6 nm (formulation T0P1) to 203.6 nm (formulation T1P1) and 221.0 nm (formulation T2P1). Finally, with double coating with Tween 80 and PEG 20000 up to 2%, mean particle size of the double-coated formulations increased from 154.5 nm (formulation T0P0) to 203.6 nm (formulation T1P1) and 276.2 nm (formulation T2P2). This could be attributed to the presence of Tween 80 facilitating the hydrogen bond formation with incoming PEG 20000 as a double coating, forming a layer-wise coherent coating over doxorubicin-loaded PBCA-NPDS (148). On the other hand, the mean particle size slightly increased from 256.9 nm (formulation T1P2) to 276.2 nm (formulation T2P2). Therefore, it can be concluded that an overcoating with high molecular weight of PEG may impact the particle size of doxorubicin-loaded PBCA-NPDS. Additionally, a low PDI value  $< 0.2$  was observed for all formulations (Table 2). This could be attributed to serial filtration step employed during the preparation and isolation of nanoparticles from reaction medium. A low PDI ( $\leq 0.2$ ) is generally deemed acceptable when selecting polymeric nanoparticles as a delivery system (149).

The mean zeta potential of placebo was observed to be -3.09 mV and for different formulations zeta potential values varied from 2.72 to 5.29 mV (Table 2). PBCA-NPDS have an inherent negative zeta potential, due to the resonance



stabilized negative charge formed during the polymerization step (150). Interestingly, the zeta potential of uncoated doxorubicin loaded PBCA-NPDS (formulation T0P0) showed a positive shift in zeta potential following the addition of doxorubicin as compared to the blank PBCA-NPDS (3.13 mV vs. -3.09 mV). This shift in the zeta potential of formulations can be attributed to the predominant positive charge of doxorubicin ( $pK_a = 8.2$ ) at a pH of 3.00 used during the polymerization reaction. No significant change in zeta potential values were observed in the presence of single- or double-coating of doxorubicin-loaded PBCA-NPDS. This finding suggests that the coating did not impact the shear plane of the particle, which otherwise would have resulted in shifts in zeta potential values.

As displayed in Table 2, the entrapment efficiency of doxorubicin within various doxorubicin-loaded PBCA-NPDS formulations varied from 86.5% (formulation T2P1) to 89.9% (formulation T0P0). A higher entrapment of doxorubicin (i.e., >86%) could be attributed to adding doxorubicin during the polymerization step. Doxorubicin when added during the polymerization step may act as a nucleophile and can form a part of the growing polymeric chain, yielding higher entrapment within the formed nanoparticles (151).

Based on Figure 7,  $^1\text{H}$  NMR spectrum comparison reveals that the amine group of doxorubicin is unconjugated with the PBCA during the formation of nanoparticle. This is based on the observed multiplet splitting at a chemical shift of about 2 ppm for both doxorubicin-loaded PBCA-NPDS (Figure 7A) and doxorubicin (Figure 7B), respectively. As reported, a multiplet splitting of the

peak at 2 ppm is a characteristic of doxorubicin which represents protons of the amine group and aliphatic carbon atom (152).

### **5.3. In vitro drug release**

#### **5.3.1. Screening of dialysis membrane**

The diffusion profile of free doxorubicin in solution across dialysis membrane with different MWCOs is shown in Figure 8. The mean cumulative doxorubicin diffused was 94.503% across the membrane (1000 KDa) as compared to 91.093%, 86.543%, and 90.523% across the membrane with 50, 100, and 300 KDa, respectively. Among various methods to study the drug release from various nano-formulations (liposomes, nanoparticles, etc.), usage of the dialysis membrane bag has been reviewed in the literature (131). However, the selection criteria of a dialysis membrane bag over another is seldom reported. Therefore, the screening of various types of dialysis membrane bags and its impact on the diffusion rate of doxorubicin through the dialysis membrane bags was performed, prior to in vitro drug release study. Although maximum amount of doxorubicin diffused across the dialysis membrane bags (MWCO: 1000 KDa) over a period of 6 hours. These results indicate that there is a delay in drug diffusion involved when using dialysis membrane bags for drug release study. Furthermore, an incomplete diffusion (i.e., <100%) indicates that even using the highest MWCOs, which is generally assumed to facilitate diffusion of free drug, may lead to an underestimation of actual drug release from the nano-formulations. Since highest amount of drug diffused across the dialysis membrane with MWCOs 1000 KDa, it was chosen for all future experiments.

### 5.3.2. In vitro drug release study of various doxorubicin loaded PBCA-NPDS

The in vitro drug release profile of all formulations is shown in Figure 9. All formulations showed characteristic biphasic release with an initial burst release followed by a second phase with a much slower rate of drug release. The initial burst release phase could be attributed to immediate desorption of doxorubicin from the surface of PBCA-NPDS. And, the next slow phase could be attributed to slow desorption of doxorubicin located in the interior of PBCA-NPDS and/or erosion of PBCA-NPDS (153). The highest amount of drug release (i.e., 78.2%) at 72 h of release study was obtained from formulation T0P0. With 2% coating of PEG 20000 (formulation T2P2), the release rate was lowest and was reduced to 35.7% over the same period of time. On the other hand, the release profile of doxorubicin was different for each formulation suggesting that doxorubicin had to diffuse through the polymer and surfactant coating employed on the doxorubicin-loaded PBCA-NPDS. A trend of decrease in release rate with the increase in Tween 80 or PEG 20000 coating concentration was observed. The amount of doxorubicin release decreased from 62.5% (formulation T1P0) to 47.5% (formulation T1P1). Similarly, the amount of doxorubicin release decreased from 59.4% (formulation T0P1) to 47.5% (formulation T1P1). Based on this trend, it can be suspected that the outward release of entrapped doxorubicin could be a function of coating concentration of PEG 20000, and not so much with Tween 80. This action of high MW PEG (typically >5000 Da) could be due to the folding of long chains of PEG. And, such folding may result in unfavorable entropy changes, which further results in compression and stability

of the coating layer (82). An existence of a similar sort of “release barrier” caused by increased concentration of PEG 20000 which is impeding the drug release is suspected. However, further surface analysis of these doxorubicin loaded PBCA-NPDS is needed to conform the existence of such a “release barrier”.

#### **5.4. Drug leakage study in FaSSIF and serum**

The drug leakage in FaSSIF and serum from various doxorubicin loaded PBCA-NPDS is shown in Figure 10. As shown in Figure 10A, the mean % doxorubicin leakage in FaSSIF after 12 hours of incubation from various doxorubicin loaded PBCA-NPDS formulations varied from 18.9-28.6%. A trend of reduction in drug leakage due to PEG 20000 overcoat was observed. Mean doxorubicin leakage reduced from 21.0% (formulation T0P0) to 18.9% (formulation T0P1). Similarly, mean doxorubicin leakage reduced from 26.8% (formulation T1P0) to 24.5% (formulation T1P1), and further reduced to 20.8% (formulation T1P2). Conversely, drug leakage increased with increase in coating with Tween 80. Mean doxorubicin leakage increased from 21.0% (formulation T0P0) to 26.8% (formulation T1P0). Similarly, mean doxorubicin leakage increased from 24.5% (formulation T1P1) to 28.7% (formulation T2P1).

As shown in Figure 10B, the highest mean leakage of doxorubicin (i.e., 3.5%) was observed in formulation T0P0. A trend of reduction in leakage with an overcoating with PEG 20000 was observed. The mean doxorubicin leakage reduced from 2.2% (formulation T1P0) to 0.3% (formulation T1P1). Further with an overcoat with Tween 80 (i.e., double-coated formulations) had a better protection efficacy towards unwanted drug leakage. A significant reduction ( $p <$

0.001) in doxorubicin leakage was observed in formulation T2P2 in comparison to single- and un-coated formulations.

The preventing of the drug leakage from double-coated doxorubicin-loaded PBCA-NPDS was observed to be resulted from the overcoating with PEG 20000. Such protective action is in line with previously published literature (154). Therefore, to maximize the protective efficacy of PEGs, and brain targeting potential with an overcoat with Tween 80, formulation T2P2, representing the highest amount of Tween 80 and PEG 20000 was selected for further exploration in in vitro cell culture model and for its biodistribution and pharmacokinetic studies in rats.

## **5.5. In vitro model to elucidate the brain uptake mechanism**

### **5.5.1. Uptake mechanism elucidation using specific inhibitors as a pretreatment**

Figure 11 illustrates the effect of various inhibitors on doxorubicin uptake from double-coated doxorubicin-loaded PBCA-NPDS (formulation T2P2) and doxorubicin solution (control). It can be observed that when bEnd.3 cells were pretreated with the growth media (no pretreatment), the mean amount of doxorubicin absorbed by cells treated with formulation T2P2 was found to be the highest (i.e., 2.6  $\mu\text{g}$ ). On the other hand, when the cells were pretreated with various inhibitors (i.e., sucrose, sodium azide, at 4°C, dynasore, and ammonium chloride) known to inhibit specific cell uptake processes, significant reduction ( $p < 0.001$  in all cases) in absorption of doxorubicin by bEnd.3 cells was observed. There are distinct internalization mechanisms for nanoparticles to enter cells

(155). In general, they can be divided into active and passive mechanism. Generally nanoparticles are internalized by the cells via energy dependent endocytosis which is influenced by temperature (such as at 4°C) under in vitro condition (156). On the other hand, free drug is internalized via passive mechanism. Therefore, several specific endocytic inhibitors to identify the internalization pathways involved in the cellular uptake of formulation T2P2 by bEnd.3 cells was evaluated in this study. Based on Figure 11, it is possible to see the effect of each inhibitor on the doxorubicin internalization from formulation T2P2 in comparison to doxorubicin solution. The uptake of doxorubicin from formulation T2P2 was found to be inhibited at 4 °C and with pretreatment with sodium azide, suggesting that their uptake was mediated by endocytosis. More specifically, involvement of clathrin-mediated endocytosis was confirmed when reduction in cell uptake doxorubicin from formulation T2P2, after pretreatment of the cells with sucrose, was observed. A reduction in cell uptake of doxorubicin from formulation T2P2, after pretreatment of the cells with dynasore, further confirmed that Tween 80 coated PBCA-NPDS may mimic as low-density lipoprotein (LDL) particles. In contrast, amount of doxorubicin absorbed by the bEnd.3 cells remained relatively similar to that of without any pretreatment when the cells were treated with doxorubicin solution (3.03 µg vs. 2.89 µg, 3.01 µg, 2.99 µg, 3.03 µg, and 2.49 µg, respectively), since the free drug is up taken by cells solely by passive absorption mechanism (157). Upon inhibiting the specific transporters, no significant reduction in the amount of doxorubicin absorbed by the cells was observed. Therefore, the main mechanism involved in the uptake of

formulation T2P2 by bEnd.3 cells was found to be LDL receptor-mediated endocytosis. In fact, LDL receptor was found to be associated with clathrin-coated pits on the cell surface, which when bound to LDL mimicking particles form clathrin-coated vesicles in the cell (158). Finally, reduction in cell uptake of doxorubicin from formulation T2P2, after pretreating with ammonium chloride, suggests that formulation T2P2 may partially follow both lysosomal and endosomal trafficking inside bEnd.3 cells, which is important for drug delivery or drug transport through barriers (159). In fact, the lysosomal pathway is responsible for nanoparticle degradation and subsequently release of drug content inside cells, while the endosomal trafficking may be involved in the transport of intact drug-loaded nanoparticles across the cell barrier. Furthermore, no cellular toxicity (i.e., mean cell viability > 85%, n = 6) was observed when the cells were incubated with various inhibitors at concentration levels described previously.

### **5.5.2. Permeability screening study**

To verify the transcytosis of formulation T2P2 transport across the monolayer on Transwell® from apical to basolateral was evaluated. The  $P_{app}$  values obtained after transport experiment of formulation T2P2 in comparison to doxorubicin solution were shown in Figure 12. The  $P_{app}$  (apical to basolateral) of doxorubicin across the monolayer was significantly higher ( $p = 0.003$ ), when the monolayer was incubated with formulation T2P2 vs. doxorubicin solution ( $9.6 \times 10^{-5}$  cm/sec vs.  $6.6 \times 10^{-5}$  cm/sec). This outcome probably happened from the interaction between ApoE adsorbed on the surface of formulation T2P2 and LDL receptors expressed on bEnd.3 cells. On the other hand, formulation T2P2

mediated transport of doxorubicin from basolateral to apical was lower (i.e., mean  $P_{app}$  of  $5.9 \times 10^{-5}$  cm/sec vs.  $1.2 \times 10^{-4}$  cm/sec) of doxorubicin solution. In general, efflux ratio [i.e.,  $P_{app}$  (apical to basolateral)/ $P_{app}$  (basolateral to apical)] is used as a first indication of involvement of active processes. Efflux ratio obtained from the mean  $P_{app}$  values of formulation T2P2 and doxorubicin solution was observed to be 0.6 and 1.8, respectively. Furthermore, a 3-fold reduction in doxorubicin mediated efflux ratio was observed by formulation T2P2 from basolateral to apical side of the monolayer. This finding is in line with the inhibitory action of Tween 80 on efflux transporters reported elsewhere (160).

## **5.6. Biodistribution and pharmacokinetic studies in rats**

### **5.6.1. Biodistribution studies**

As shown in Figure 13, significant amount ( $p = 0.017$ ) of doxorubicin was available in the serum after 3 hours following oral administration of formulation T2P2 (Figure 13A) at a dose of 70 mg/kg (group 3). This could be due to the higher circulation time yielded by coating with PEGs. Higher circulation time may have resulted in increased drug available in the circulation from the formulation T2P2. Furthermore, no significant difference was observed in doxorubicin availability in serum among other groups. Comparing the mean values, it can be observed that the maximum amount of doxorubicin was available in serum after oral administration of doxorubicin solution (Figure 13A). Based on Figure 13B, significant brain accumulation of doxorubicin occurred after 1 hour following oral administration of formulation T2P2 at dose level of 70 mg/kg (group 3) in comparison to formulation T2P2 at dose level of 50 mg/kg ( $p =$



0.005) (group 2) and doxorubicin solution at dose level of 70 mg/kg ( $p = 0.017$ ) (group 4). These findings are in line with our previous studies, wherein the maximum anti-nociceptive effect was achieved with the highest dose of formulation T2P2 after 60 minutes of oral administration (6). Also, as expected, although insignificant, higher brain accumulation of doxorubicin occurred after intravenous administration and a trend of exposure-time relationship was observed. Based on Figure 13C, as expected, significant accumulation of doxorubicin occurred in liver after 1 hour following intravenous or oral administration of formulation T2P2 ( $p = 0.027$ ) (groups 1-3) in comparison to doxorubicin solution (group 4). This situation can be summarized by suggesting that the liver acts as a reservoir of doxorubicin-loaded PBCA-NPDS, facilitating their rapid first-phase disappearance from the blood and their second-phase release in the body under degraded and/or excretable forms (151). Intrahepatic distribution studies demonstrate that Kupffer cells are the major liver site of accumulation of PACA nanoparticles (161). And, endocytosis plays a major role in the uptake process of these nanoparticles (162). Once up taken by the liver, nanoparticles may have metabolized with a sustained release of the drug from tissues, which is in agreement with previously published reports on PBCA-NPDS as drug carriers (163,164). Since this investigation using an in vitro cell culture model also demonstrated involvement of endocytosis mechanism. The same processes involved in the fate of the formulation T2P2 in liver was suspected. On the other hand, doxorubicin solution was rapidly degraded and eliminated from

the body, which further verify the findings from the pharmacokinetics studies to be described below.

### **5.6.2. Pharmacokinetic studies**

Figure 14 illustrates the observed and the fitted pooled serum doxorubicin concentration-time curves of formulation T2P2 obtained after simultaneous model fitting. As shown in Figure 14A and 14B, the serum doxorubicin concentration-time profiles, after intravenous and oral administration of formulation T2P2, were adequately fitted by the 2-compartment model (Equations 3 and 4). On the other hand, 2-compartment model was not operative for describing the data obtained after oral administration of doxorubicin solution. This could be attributed to the faster clearance of the doxorubicin from the circulation as observed from the rapid decline of the serum concentration (Figure 14A). Comparison of the dosage-form related parameters (i.e., absorption rate and lag time of absorption), formulation T2P2 exhibited a higher absorption rate of  $0.05 \text{ min}^{-1}$  and  $0.08 \text{ min}^{-1}$  at 50 mg/kg and 70 mg/kg, respectively. On the other hand, the absorption rate of doxorubicin solution was found to be  $0.003 \text{ min}^{-1}$ . This could be due to the absorption enhancement efficacy of the formulation T2P2. Furthermore, the lag time of absorption value of formulation T2P2 was higher (i.e., 3.3-fold) as compared to that of doxorubicin solution. A higher lag time of absorption value obtained by formulation T2P2 indicates a delayed absorption of the formulation. This can be attributed to an intrinsic delay in nanoparticles entry into the lymphatics (165). Reliability of the estimated parameters were determined by comparing the magnitude of the coefficient of variance associated with the parameters. Although

there are no magic cut-offs, a lower value of coefficient of variance is sought for determining the reliability of the parameter estimates. A comparatively higher coefficient of variance associated with doxorubicin solution could be due to the inability of the 2-compartment to explain the observed data.

### **5.7. In vitro cell culture studies**

To investigate the uptake of double-coated doxorubicin-loaded PBCA-NPDS, intracellular accumulation of doxorubicin within SW620 cells, based on its characteristic red fluorescence, was determined, and shown in Figure 15. And, for the comparison of outcomes shown in Figure 15, the corresponding corrected total cell fluorescence values, are calculated and represented in Figure 16.

As shown in Figure 15, doxorubicin-associated fluorescence occurred mainly in the nuclei of the SW620 cell line for all doxorubicin-loaded PBCA-NPDS formulations (Figure 15a-g) and free doxorubicin (Figure 15h). Based on the calculated corrected total cell fluorescence values shown in Figure 16, a trend of increase in mean fluorescence intensity with an increase in the concentration of Tween 80 was observed. Formulation T2P2 significantly increased ( $p < 0.001$ ) increased the accumulation of doxorubicin in comparison to formulations T1P1 and T2P1. Furthermore, no significant difference was observed in the fluorescence intensity between formulation T2P2 and free doxorubicin solution. This finding could be attributed to the sensitivity of the cell line toward treatment with doxorubicin. Since SW620 cells do not overexpress P-gp transporters, doxorubicin could readily access the cells and the rate of drug efflux is also reduced.

In addition to the SW620 cell line, intracellular accumulation of various doxorubicin-loaded PBCA-NPs formulations were performed with the AD300 cell line. The characteristic red fluorescence and corresponding corrected total cell fluorescence values are shown in Figure 17 and 18, respectively. Similarly, to SW620 cells, all doxorubicin-loaded PBCA-NPs formulations resulted in increased fluorescence intensity within AD300 cells (Figure 17a-g). On the other hand, as expected, no nuclei accumulation was observed, when cells were treated with free doxorubicin. Instead, the fluorescence signal was observed on the cell membranes (Figure 17h). This could be due to over-expressed P-gp on AD300 cells, which did not allow doxorubicin accumulation in the nuclei (166). In comparison, the intracellular localization of doxorubicin in AD300 cells treated with formulations T2P1 (Figure 17f), and T2P2 (Figure 17g) exhibited the highest intensity. As shown in Figure 18, formulation T2P2 exhibited the significantly higher ( $p < 0.001$ ) intensity as compared to formulations T0P1, T1P0, T1P1, T1P2 as well as free doxorubicin, indicating enhanced retention of doxorubicin within AD300 cells. These findings are in line with the inhibitory action of Tween 80 on over-expressed P-gp receptors due to the higher drug retention within AD300 cells.

The cytotoxicity profiles of doxorubicin-loaded PBCA-NPs formulations from MTT assays performed on SW620 and AD300 cell lines are illustrated in Figure 19 and 20, respectively. For the comparison of the cytotoxicity profiles,  $IC_{50}$  values (i.e., half-maximal inhibitory concentration) were calculated and displayed in Table 3. The  $IC_{50}$  values of free doxorubicin in SW620 and AD300

cell lines were 0.094  $\mu\text{M}$  and 4.796  $\mu\text{M}$ , respectively. Interestingly, it was observed that double-coated doxorubicin-loaded PBCA-NPs (specifically formulation T2P2) showed significantly higher ( $p < 0.001$ ) cytotoxicity than free doxorubicin, single-coated (formulation T0P1) ( $p < 0.001$ ), and un-coated (formulation T0P0) ( $p = 0.004$ ) in AD300 cell line. These results suggest that double-coated PBCA-NPs, specifically, formulation T2P2 have improved anticancer property in doxorubicin resistant AD300 cells. A trend of higher cytotoxicity with increased concentration of coating with Tween 80 was observed. This trend could be attributed to inhibition of overexpressed p-glycoprotein transmembrane receptors by Tween 80 as previously reported. On the other hand, synergistic effect on cytotoxicity in AD300 cell line was observed with double-coated doxorubicin-loaded PBCA-NPs with Tween 80 and PEG 20000. Trend analysis of the synergistic effect indicates that overcoating with PEG 20000 might aid in partial reversal of resistance, which could be attributed to folding of high molecular weight PEG ( $> 5000$  Da) presenting a barrier comprising of conformationally random molecular chains to prevent drug efflux. This partial resistance reversal action of doxorubicin-loaded PBCA-NPs formulations was determined by calculating the resistance fold (i.e., ratio of  $\text{IC}_{50}$  values obtained in AD300 cells to those obtained in SW620 cells). As shown in Table 3, a reduction in doxorubicin mediated resistance on AD300 cell line treated with formulation T2P2 as compared to doxorubicin solution was identified (22.445-fold versus 51.020-fold) indicating that double-coating with Tween 80 and PEG 20000 on PBCA-NPs may potentiate the sensitivity of the resistant cells towards

doxorubicin. However, no significant change in IC<sub>50</sub> values was observed when SW620 cells were treated with free doxorubicin in solution or formulation T2P2. This is based on the assumption that, incorporating doxorubicin within the nanoparticle will not impact its efficacy. Since IC<sub>50</sub> is a drug related parameter, we anticipate it to be similar.

The cytotoxicity profiles of doxorubicin-loaded PBCA-NPs formulations from MTT assays performed on H460 and BCRP-overexpressed MX20 cells are shown in Figure 21 and 22, respectively. And, IC<sub>50</sub> values were calculated and compared in Table 4. The IC<sub>50</sub> values of free doxorubicin within H460 and MX20 cell lines were 0.058  $\mu$ M and 0.813  $\mu$ M, respectively. It was observed that double-coated doxorubicin-loaded PBCA-NPs (formulation T1P1) showed significantly higher ( $p < 0.001$ ) cytotoxicity (about 1-fold) than free doxorubicin in comparison to single-coated PBCA-NPs (formulation T0P1) resulting in partial reversal by about 3.5-fold. These results suggest that these double-coated PBCA-NPs formulations might have improved anticancer property in mitoxantrone resistant MX20 cells. A similar trend (with respect to SW620 and AD300 cells) of higher cytotoxicity with increased concentration of overcoating with Tween 80 was observed. Consequently, formulation T2P2, exhibited significantly higher cytotoxicity in comparison to formulation T1P1. This finding suggests that an overcoat of Tween 80 at 2% might be required for enhanced cytotoxicity of formulations in resistant cells. Further, this trend could be attributed to inhibition of overexpressed BCRP transmembrane transports by Tween 80 as previously reported (167). On the other hand, synergistic effect on cytotoxicity in MX20 cell

line was observed with double coating of doxorubicin-loaded PBCA-NPs formulations with Tween 80 and PEG 20000. Trend analysis of the synergistic effect indicates that overcoating with PEG 20000 may also aid in partial reversal of resistance, which could be attributed to folding of high molecular weight PEG (20000 Da in this case) is presenting a barrier comprising of conformationally random molecular chains to prevent drug efflux (168). Furthermore, based on the calculated resistance fold value (Table 4), it can be observed that formulation T2P2 is also able to potentiate the sensitivity of doxorubicin in the mitoxantrone mediated resistant cell line (i.e., MX20), wherein the reduction of resistance from 13.943-fold (i.e., doxorubicin solution) to 4.851-fold was observed. However, contrary to their enhanced efficacy towards the resistant cell line, lower cytotoxicity (higher  $IC_{50}$  values) as compared to doxorubicin solution for all doxorubicin-loaded PBCA-NPs formulations was observed in H460 cell line, indicating the specificity of these formulations towards the resistant MX20 cell line. Furthermore, this difference could be attributed to variability in the availability of doxorubicin at the cellular level. For example, free doxorubicin is instantly available within the cells, whereas, with nanoparticles time dependent drug release also needs to be taken into consideration.

## **6. Conclusion**

It has been reported that an overcoat with PEG 20000 coating enhanced the stability of this formulation in the gastrointestinal tract. And, a particle size of less than 300 nm could have influenced the M-cells mediated uptake of these formulation, and its subsequent transport into the systemic circulation. On the

other hand, Tween 80 coating facilitated the adsorption of ApoE from the circulation and subsequently facilitated the brain delivery of PBCA-NPDS by LDL receptor mediated endocytic uptake across the BBB. As a result, double-coated doxorubicin PBCA-NPDS (formulation T2P2) was observed cross the gastrointestinal barrier after oral administration and still retain its targeting properties to the brain. Furthermore, under in vitro conditions Formulation T2P2, exhibited enhanced cytotoxicity and specificity towards the P-gp and BCRP overexpressing cell lines. Similar to in vivo studies the success of double-coated PBCA-NDs can be hypothesized due to interplay of a number of factors simultaneously. They could be (a) particle size less than 300 nm, and (b) double coats of Tween 80 and PEG 20000. The particle size of the formulation could have helped in endocytic uptake of the nanoparticles across the cell barrier. The action of double-coats of Tween and PEG are suspected to play the following roles. The role of Tween 80 and PEG 20000 coating had been the enhancement of accumulation of doxorubicin from double-coated PBCA-NPDS (formulation T2P2) in both P-gp and BCRP overexpressing cell lines. Hence, we can conclude that, the application of the double-coated PBCA-NPDS with overcoats of Tween 80 and PEG 20000 could be feasible approach to deliver and target doxorubicin to brain via the oral route and aid in overcoming MDR.



## 7. Tables

Table 1: Physiochemical characterization methods for nanoparticles

Parameter	Method
Particle size	Photon correlation spectroscopy, Transmission electron microscopy (TEM), Scanning electron microscopy (SEM)
Surface charge	Electrophoresis, Laser doppler anemometry
Crystallinity	X-ray diffraction (XRD), Differential scanning calorimetry (DSC)
Hydrophobicity	Hydrophobic interaction chromatography, contact angle measurement
Molecular weight determination	Gel chromatography

Table 2: Formulation codes and characteristics of various doxorubicin-loaded PBCA-NPDS. Data presented as mean  $\pm$  standard deviation, n = 3.

Formulation	Codes	Particle size (nm)	PdI	Zeta potential (mV)	% Entrapment efficiency
-	Placebo*	109.4 $\pm$ 3.3	0.083 $\pm$ 0.022	-3.09 $\pm$ 0.97	Not applicable
Core	T0P0	154.5 $\pm$ 1.4	0.044 $\pm$ 0.039	3.13 $\pm$ 0.84	89.9 $\pm$ 0.1
Single-coated	T0P1	182.6 $\pm$ 25.5	0.040 $\pm$ 0.019	2.72 $\pm$ 0.94	87.0 $\pm$ 0.1
	T1P0	154.4 $\pm$ 5.7	0.076 $\pm$ 0.028	4.19 $\pm$ 0.78	88.3 $\pm$ 0.3
Double-coated	T1P1	203.6 $\pm$ 8.1	0.064 $\pm$ 0.046	5.29 $\pm$ 2.24	88.5 $\pm$ 0.1
	T1P2	256.9 $\pm$ 9.1	0.082 $\pm$ 0.017	3.95 $\pm$ 0.84	88.5 $\pm$ 0.4
	T2P1	221.0 $\pm$ 20.0	0.129 $\pm$ 0.116	3.08 $\pm$ 2.30	86.5 $\pm$ 0.2
	T2P2	276.2 $\pm$ 15.4	0.110 $\pm$ 0.062	2.75 $\pm$ 0.48	88.4 $\pm$ 0.3

\* Placebo = PBCA-NPDS (blank nanoparticles)

Table 3: The cytotoxic effect of doxorubicin and double-coated doxorubicin-loaded PBCA-NPDS on SW620 and AD300 cell lines.

Treatment	SW620	AD300	
	IC <sub>50</sub> ± SD <sup>a</sup> (μM)	IC <sub>50</sub> ± SD <sup>a</sup> (μM)	RF <sup>b</sup>
Free doxorubicin	0.094 ± 0.018	4.796 ± 0.271	51.020
T0P0	0.061 ± 0.013	2.653 ± 0.125	43.491
T0P1	0.068 ± 0.012	2.700 ± 0.066	39.705
T1P0	0.073 ± 0.004	1.857 ± 0.464 <sup>#</sup>	25.438
T1P1	0.044 ± 0.017	1.613 ± 0.161 <sup>*</sup>	36.659
T1P2	0.081 ± 0.004	1.866 ± 0.082	23.037
T2P1	0.067 ± 0.023	1.775 ± 0.062	26.492
T2P2	0.074 ± 0.012	1.661 ± 0.142 <sup>##</sup>	22.445

IC<sub>50</sub>: concentration that inhibited cell survival by 50%

RF: Resistance fold was the ratio of IC<sub>50</sub> value from AD300 cells over SW620 cells, respectively for all treatments. <sup>\*</sup>Statistically significant ( $p < 0.001$ ) in comparison to formulation T0P1, and <sup>#</sup> $p = 0.004$  in comparison to formulation T0P0. <sup>##</sup> $p < 0.001$  in comparison to free drug, and formulation T0P0 and T0P1.

Table 4: The cytotoxic effect of doxorubicin and double-coated doxorubicin-loaded PBCA-NPDS on H460 and MX20 cell lines.

Treatment	H460		MX20
	IC <sub>50</sub> ± SD <sup>a</sup> (μM)	IC <sub>50</sub> ± SD <sup>a</sup> (μM)	RF <sup>b</sup>
Free doxorubicin	0.058 ± 0.002	0.813 ± 0.014	13.943
T0P0	0.196 ± 0.012	1.574 ± 0.097	8.019
T0P1	0.173 ± 0.012	1.597 ± 0.067	9.225
T1P0	0.112 ± 0.024	0.626 ± 0.025	5.603
T1P1	0.154 ± 0.016	0.674 ± 0.013 <sup>#</sup>	4.374
T1P2	0.189 ± 0.045	0.817 ± 0.030	4.313
T2P1	0.158 ± 0.002	0.637 ± 0.011	4.038
T2P2	0.135 ± 0.023	0.653 ± 0.005*	4.851

IC<sub>50</sub>: concentration that inhibited cell survival by 50%

RF: Resistance fold was the ratio of IC<sub>50</sub> value from MX20 cells over H460 cells, respectively for all treatments. \*Significantly lower ( $p = <0.001$ ) in comparison to formulation T1P2, and <sup>#</sup> $p = <0.001$  in comparison to formulation T0P1.

## 8. Figures

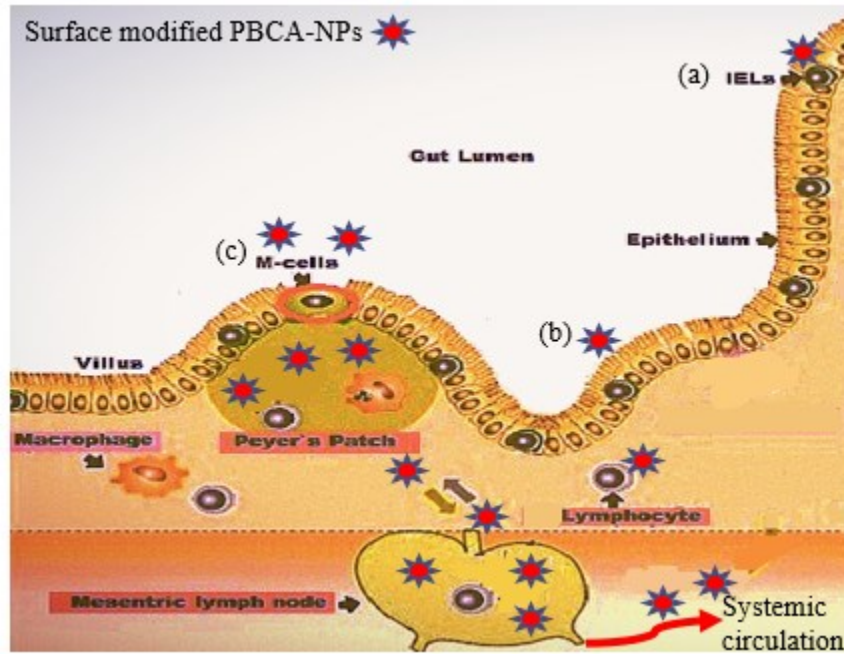


Figure 1: Schematic representation of three possible mechanisms of gastrointestinal uptake of surface modified poly(butyl cyanoacrylate) nanoparticles (PBCA-NPDS). ★ Represents surface modified PBCA-NPDS: (a) intracellular uptake (*via* intra-epithelial lymphatics, IELs); (b) intracellular/paracellular uptake; (c) uptake *via* the M-cells and Peyer's patches in the gut lumen. Adapted from reference (1) with modifications.

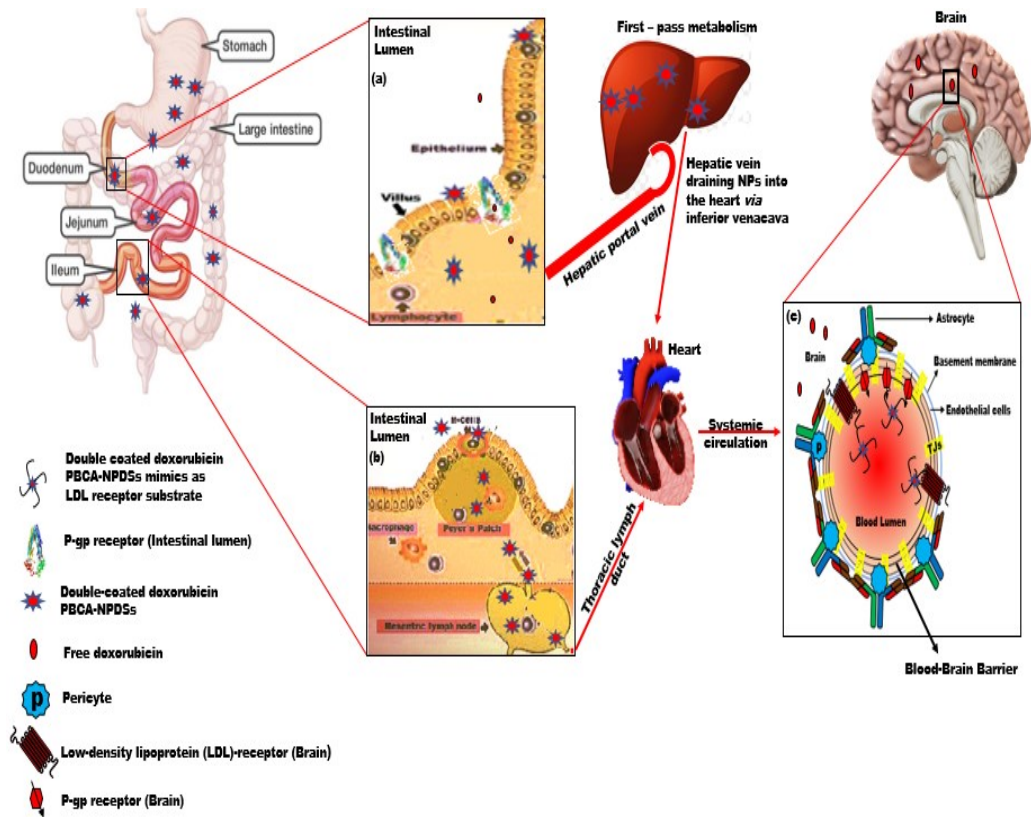


Figure 2: Schematic representation pathway of doxorubicin delivery to the brain facilitated by double-coated doxorubicin-loaded PBCA-NPDS after oral administration: (a) doxorubicin efflux in the lumen facilitated by the P-gp receptor in the duodenum following either intracellular and/or paracellular uptake by the duodenum, (b) uptake of double-coated doxorubicin-loaded PBCA-NPDS via the M-cells of the Peyer's patches of the ileum, and (c) LDL-receptor mediated transcytosis of the double-coated doxorubicin-loaded PBCA-NPDS from blood lumen into the brain.

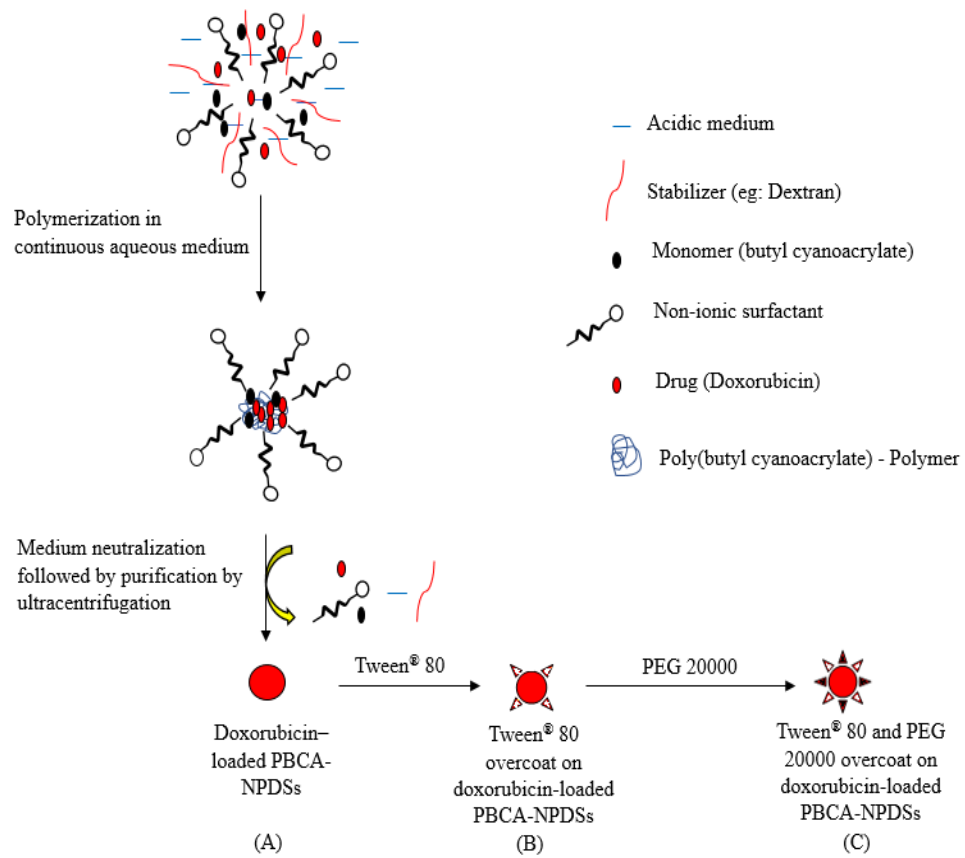


Figure 3: Schematic representation of nanoparticle formulation. (A) doxorubicin-loaded PBCA-NPDS (core), (B) Tween 80 overcoated nanoparticles, and (C) Tween 80 and PEG 20000 overcoated nanoparticles. Adapted from reference (67) with modifications.

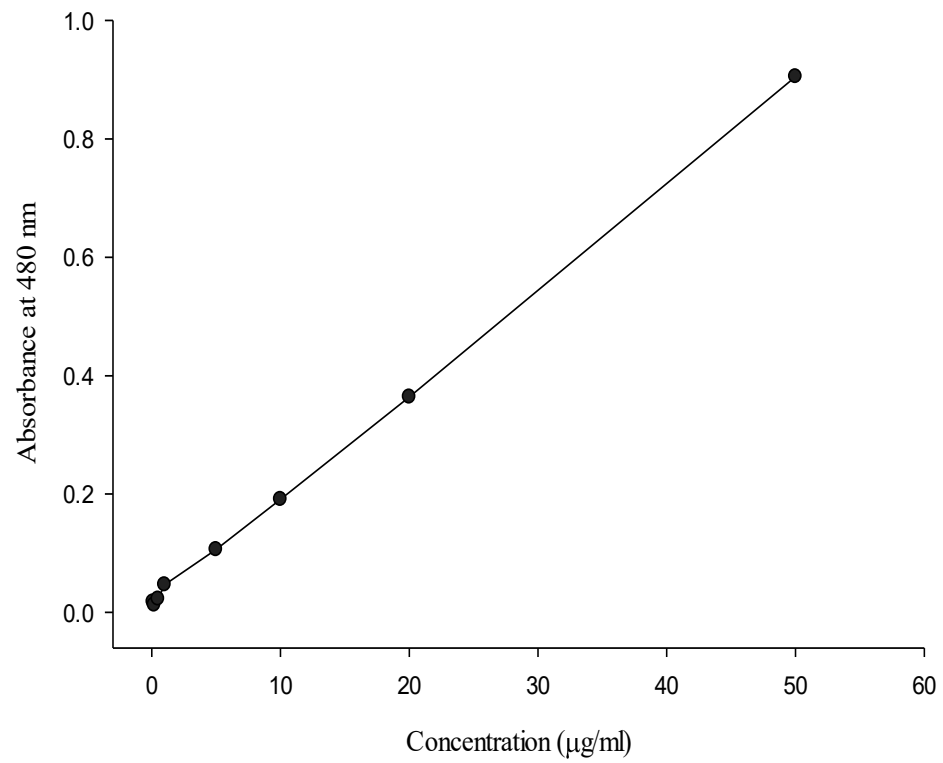


Figure 4: Calibration curve of doxorubicin assayed by the UV-Vis spectroscopy method ( $R^2 = 0.9996$ ,  $n = 6$ ).



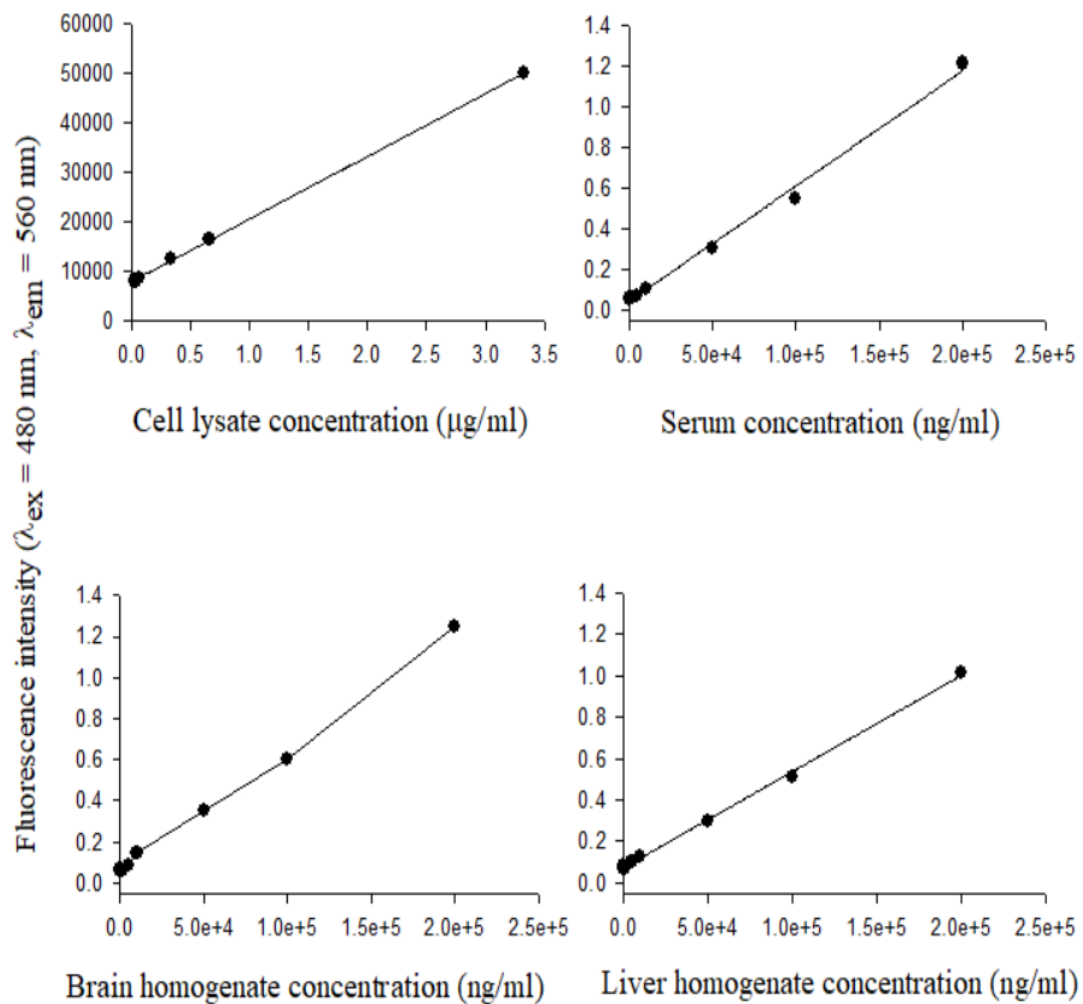


Figure 5: Calibration curve of doxorubicin assayed by the fluorescence spectroscopy (plate-reader method) spiked in various medium ( $R^2 > 0.995$  in each case ,  $n = 6$ ).

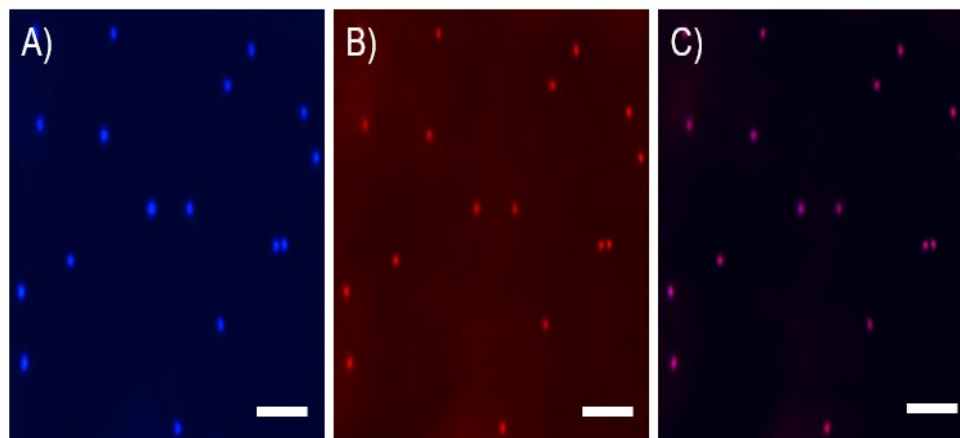
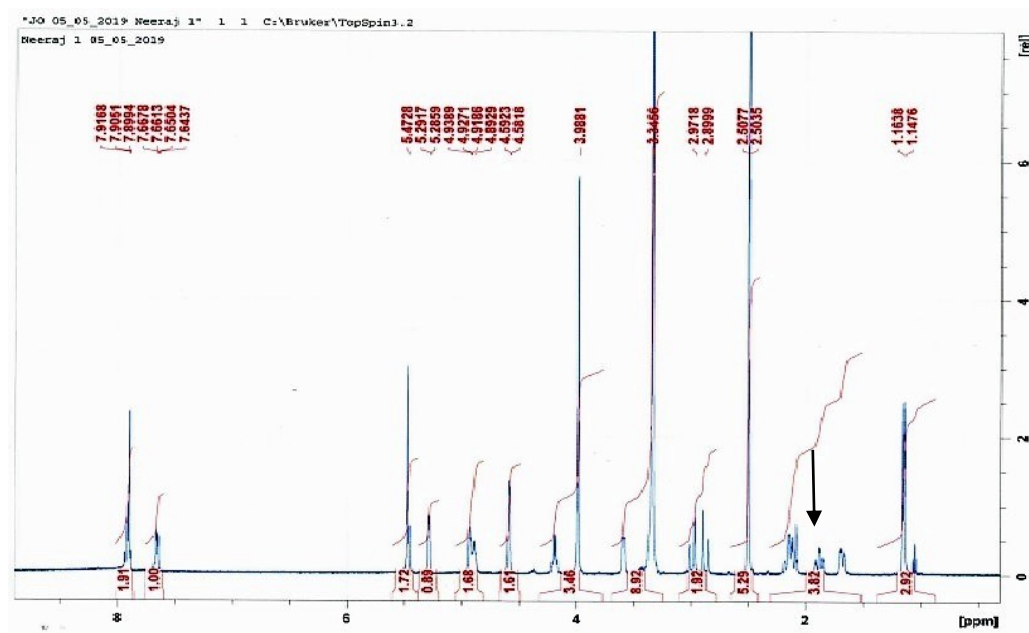


Figure 6: Fluorescence microscopy images of cells for method selection. A) cell nuclei stained DAPI, B) cells treated with free doxorubicin, exhibiting characteristic red fluorescence associated with doxorubicin within the cell, and C) merged image of the cells is depicted by an arrow. (Scale bar: 10  $\mu\text{m}$ ).

a)



b)

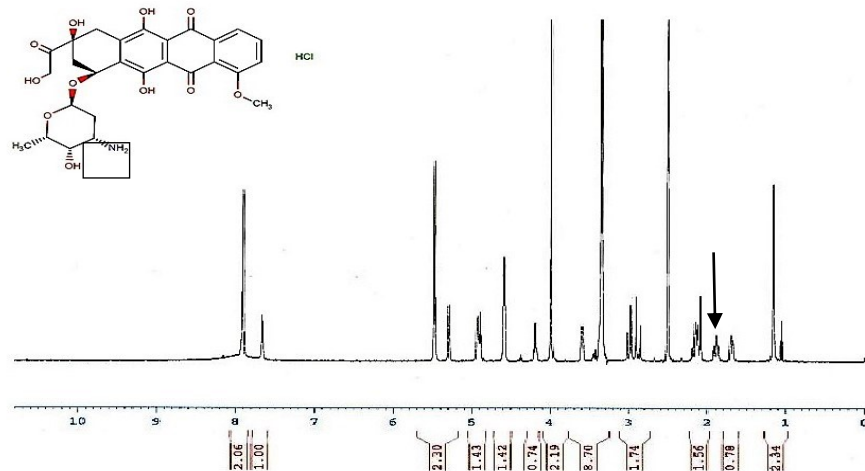


Figure 7:  $^1\text{H}$  NMR of spectrums of a) doxorubicin-loaded PBCA-NPDS, and b) free doxorubicin in  $\text{DMSO-d}_6$ . Arrow shows a characteristics peak for the protons associated with amine and aliphatic carbon atom (boxed in the chemical structure).

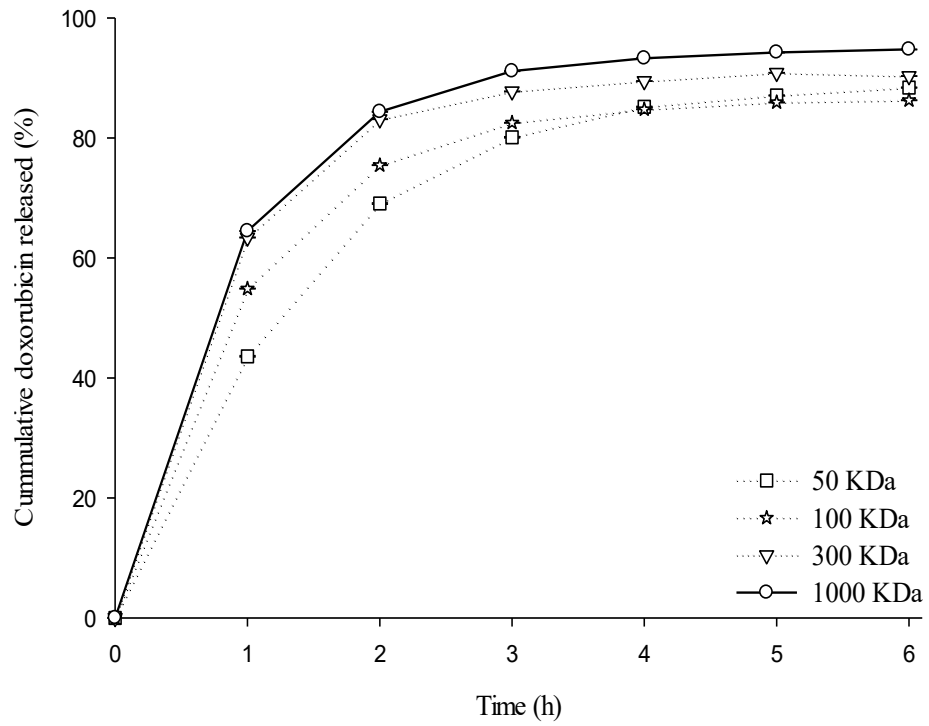


Figure 8: Comparison of diffusion profiles of free doxorubicin using different MWCO dialysis membranes in the release medium at  $37^{\circ} \pm 0.5^{\circ}\text{C}$ , 100-120 rpm. (Data are presented as mean  $\pm$  standard deviation, n = 3).

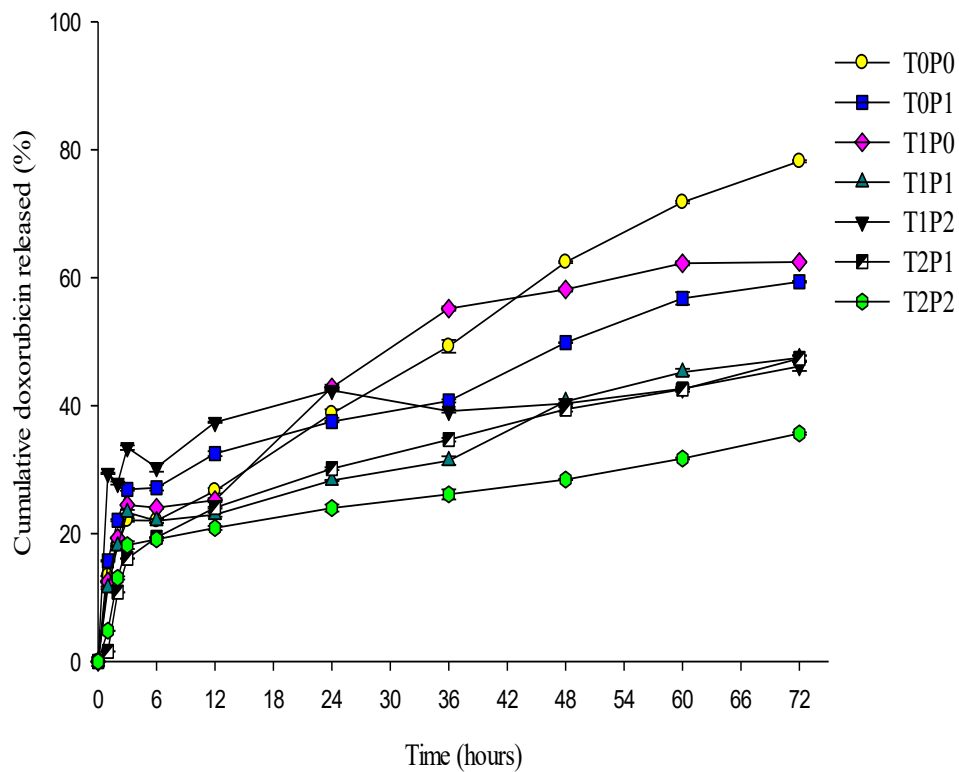
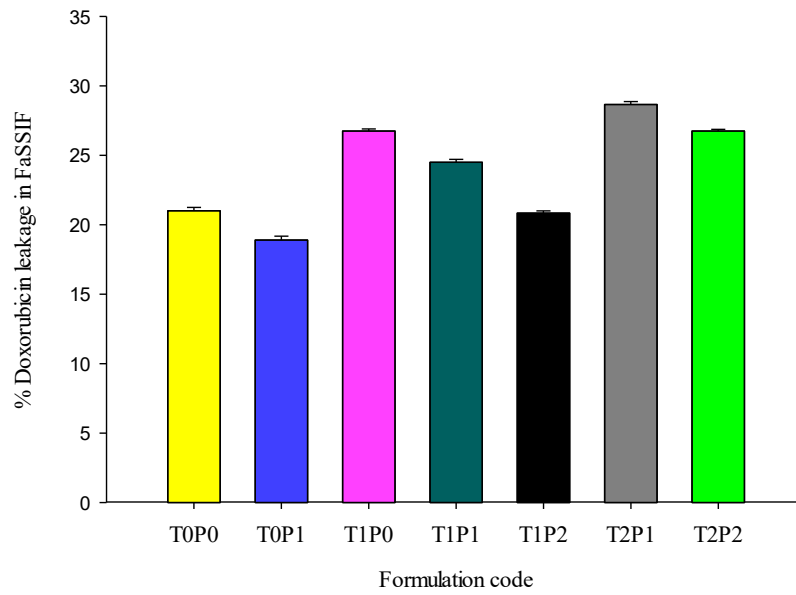


Figure 9: In vitro drug release profiles of various doxorubicin-loaded PBCA-NPDS (Data presented as mean  $\pm$  standard deviation, n = 3).

a)



b)

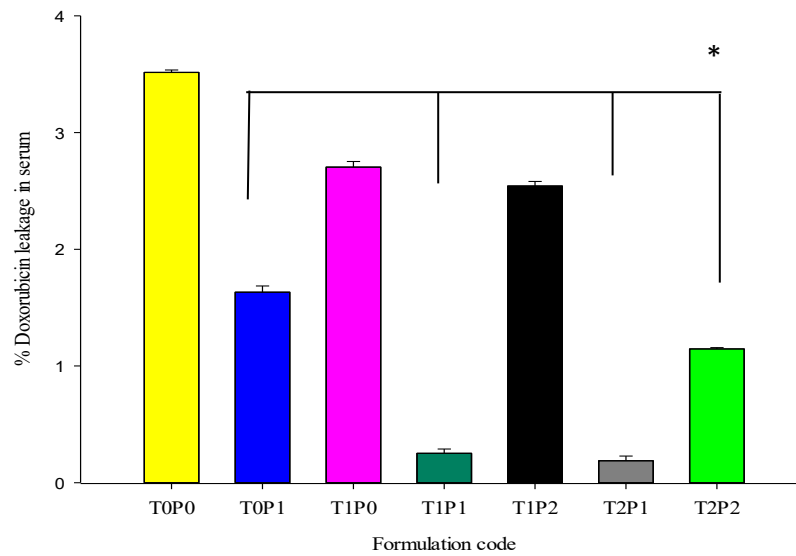


Figure 10: % Doxorubicin leakage from various doxorubicin-loaded PBCA-NPDS after 12 hours incubation period in a) FaSSIF, and b) Serum at  $37^{\circ} \pm 0.5^{\circ}\text{C}$  and 100–120 rpm. (Data presented as mean  $\pm$  standard deviation, n = 3).

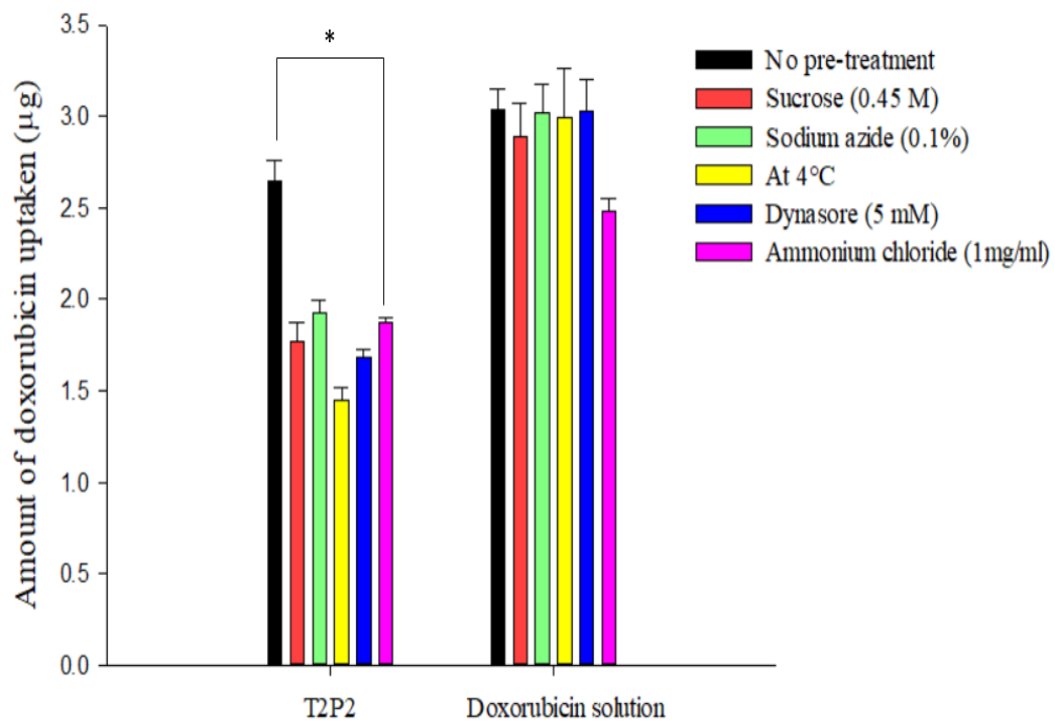


Figure 11: The in vitro model in which bEnd.3 cells were subjected to various inhibitors as pretreatments, and then followed with treatment of formulation T2P2 or doxorubicin solution for additional 3 hours of cell incubation for elucidation of the brain uptake mechanism (data presented as mean  $\pm$  standard deviation, n = 6).

\* Significantly ( $p < 0.001$ ) reduced uptake of doxorubicin in bEnd.3 cells pretreated with various inhibitors.

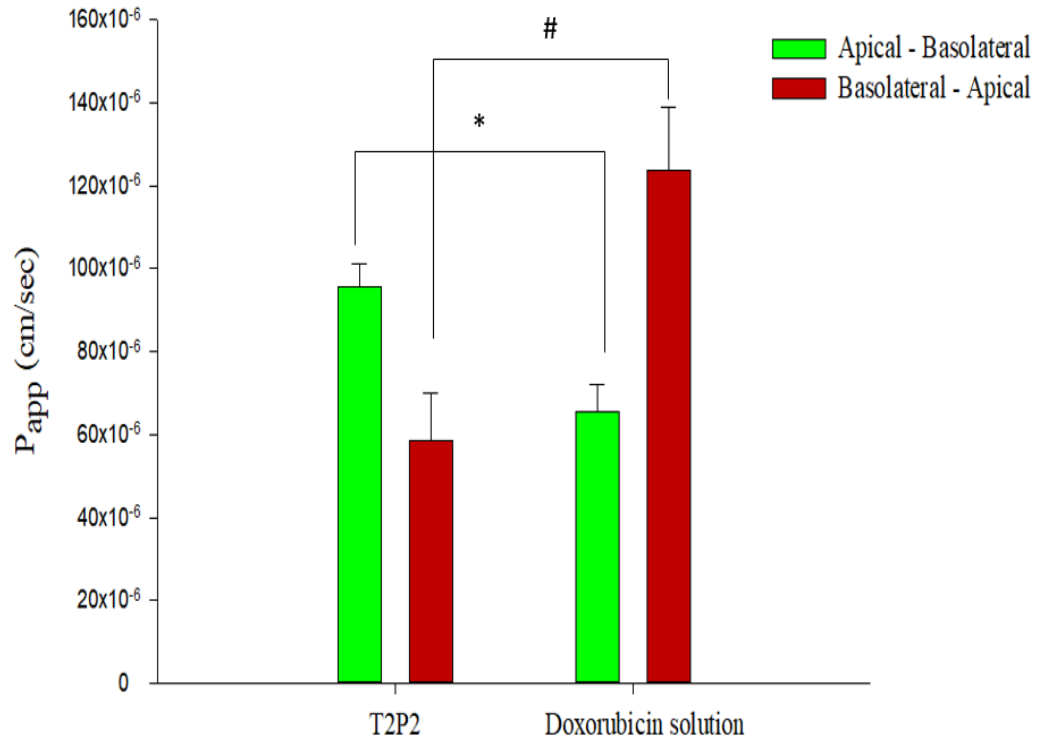


Figure 12: Apparent permeability ( $P_{app}$ ) after transport experiment of formulation T2P2 or doxorubicin solution across bEnd.3 cells monolayer after 2 hours incubation period (data presented as mean  $\pm$  standard deviation,  $n = 3$ ). \* $p = 0.003$  and # $p = 0.004$  of doxorubicin permeation (higher) and efflux (lower) mediated by formulation T2P2, from apical to basolateral and basolateral to apical side, respectively, in comparison to doxorubicin solution.



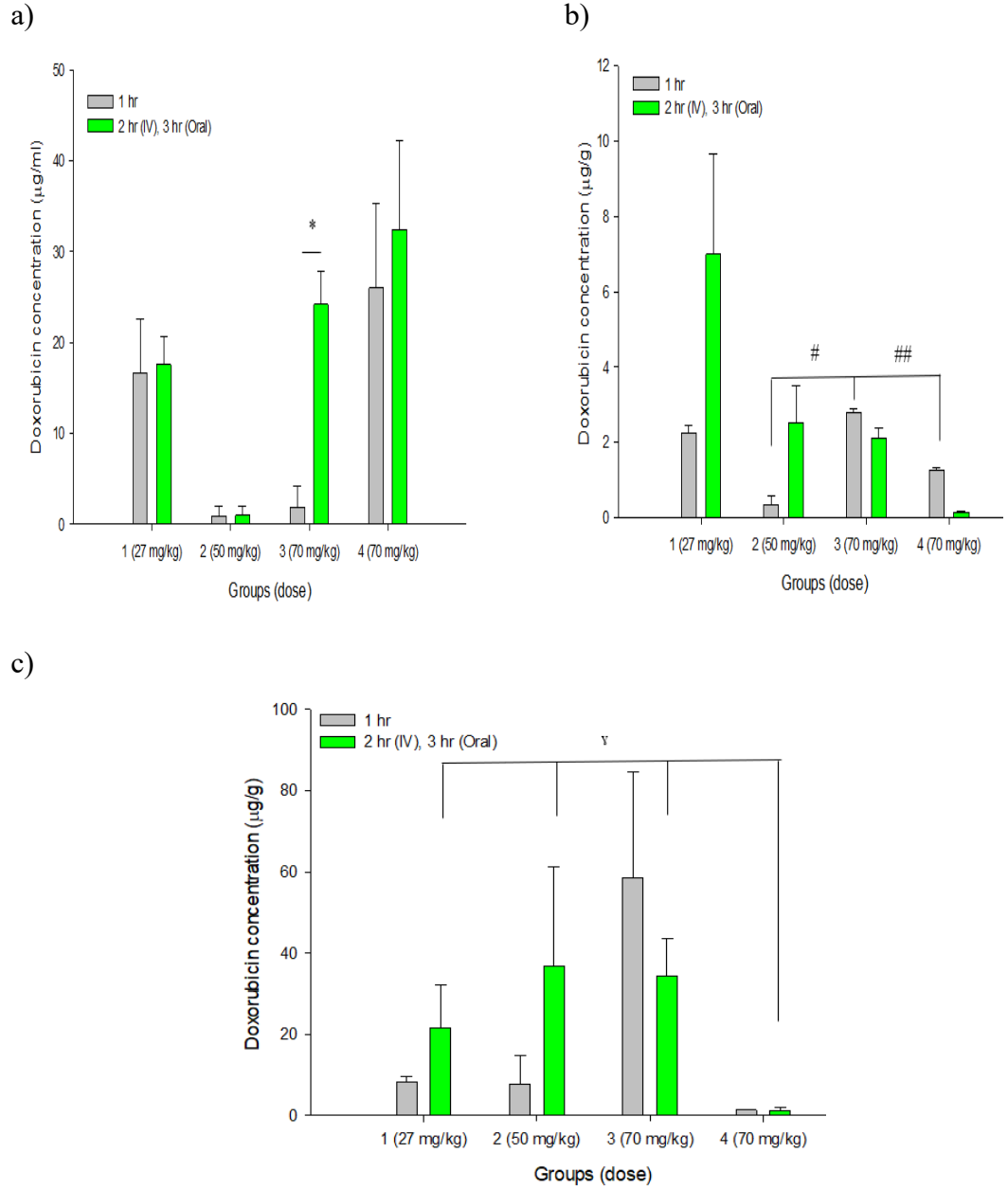
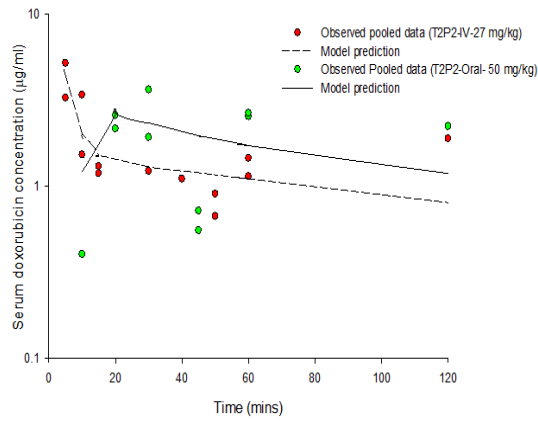
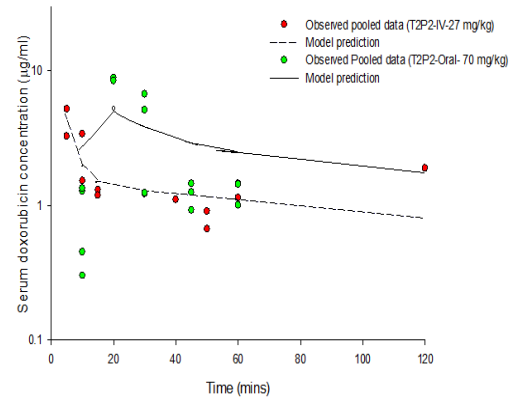


Figure 13: Biodistribution of doxorubicin in a) serum, b) brain, and c) liver from formulation T2P2 after intravenous administration (group 1) and oral administration (groups 2-3), in comparison to oral doxorubicin solution (data present mean  $\pm$  standard deviation, n = 2). \*p = 0.017 in comparison to 1 hour, #p = 0.005 in comparison to group 2 at 1 hour, ##p = 0.017 in comparison to group 4 at 1 hour, and  $\gamma$ p = 0.027 in comparison to groups 1-3 after 3 hours.

a)



b)



c)

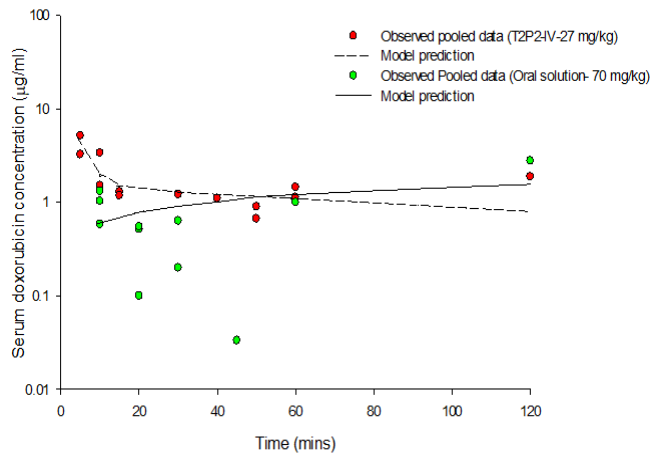


Figure 14: Simultaneous model fitting of pooled doxorubicin serum concentration-time profiles after intravenous administration of formulation T2P2 (27 mg/kg), respectively, with a) oral administration of T2P2 (50 mg/kg), b) oral administration of T2P2 (70 mg/kg), and c) oral administration of doxorubicin solution (70 mg/kg).

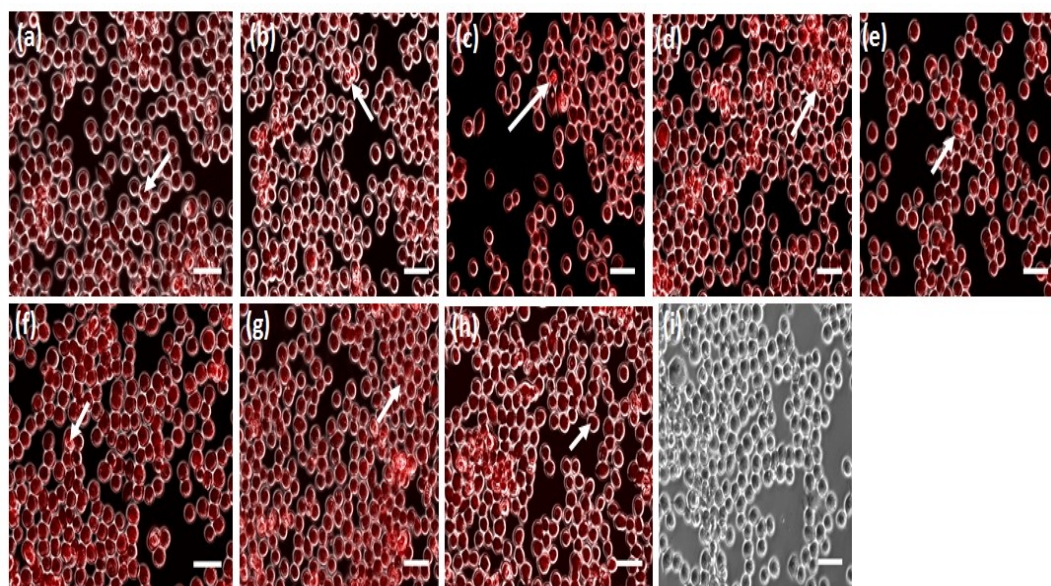


Figure 15: Fluorescence associated with intracellular accumulation of doxorubicin within human colon adenocarcinoma cell line SW620, following treatment with, (a) T0P0, (b) T0P1, (c) T1P0, (d) T1P1, (e) T1P2 (f) T2P1, (g) T2P2, (h) Free doxorubicin, and (i) No treatment. Note: Arrows represent the accumulation of doxorubicin in the nucleus. (Magnification: 40 $\times$ , Scale bar: 10  $\mu$ m).

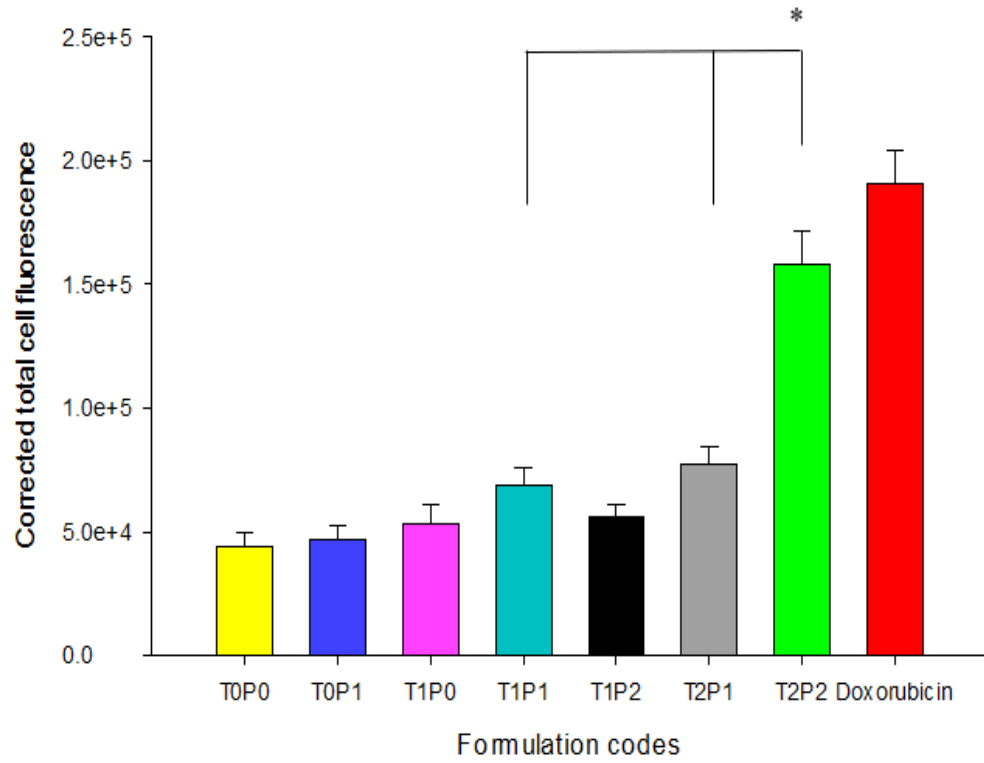


Figure 16: The values of calculated corrected total cell fluorescence intensity within SW620 cells, based on the outcomes shown in Figure 15 (data presented as mean  $\pm$  standard deviation, number of cells counted = 50, \*p = < 0.001).

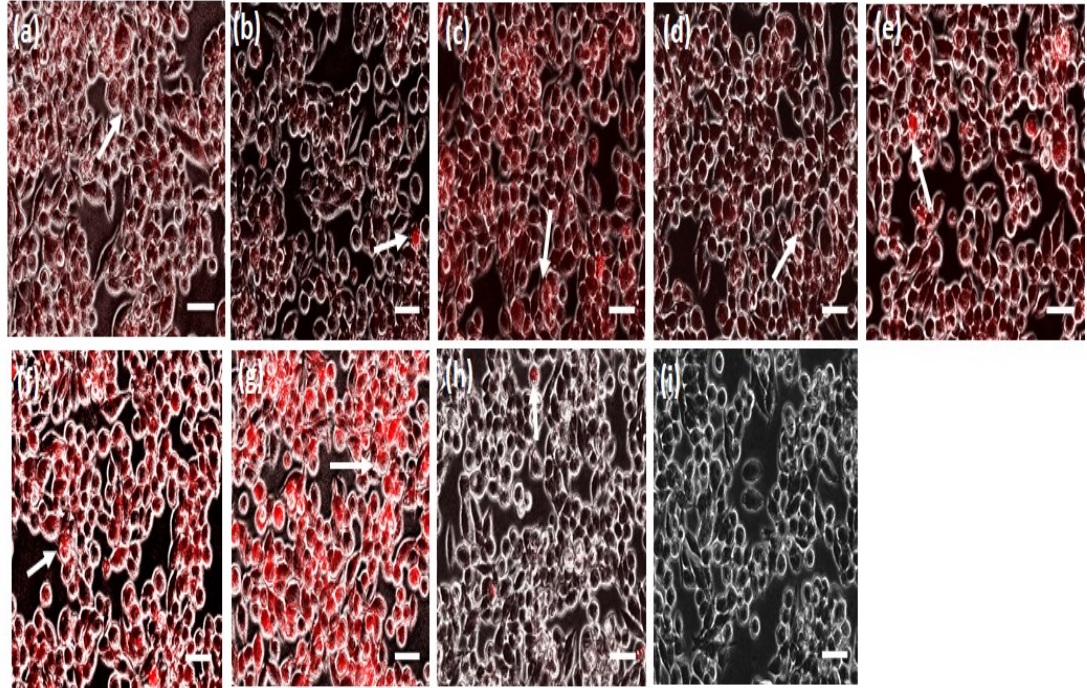


Figure 17: Fluorescence detection upon the intracellular accumulation of doxorubicin in doxorubicin-resistant human colon adenocarcinoma cell line AD300, following treatment with, (a) T0P0, (b) T0P1, (c) T1P0, (d) T1P1, (e) T1P2 (f) T2P1, (g) T2P2, (h) Free doxorubicin, and (i) No treatment. Arrows represent the accumulation of doxorubicin in the nucleus. (Magnification: 40 $\times$ , Scale bar: 10  $\mu$ m).

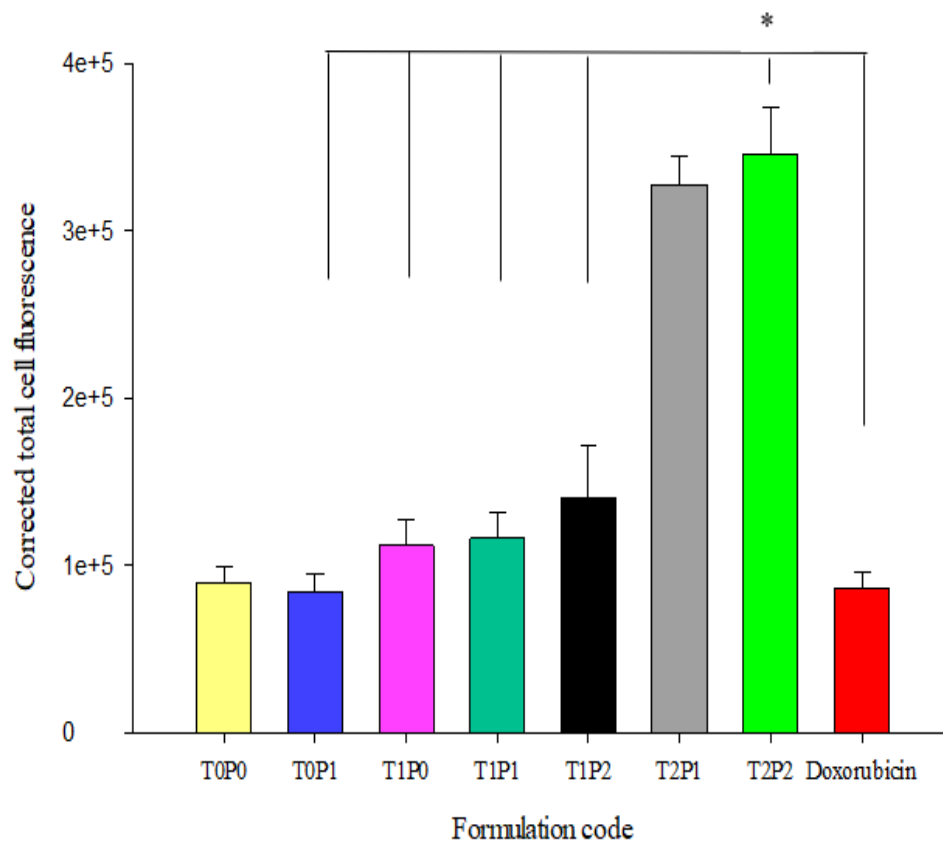


Figure 18: The values of calculated corrected total cell fluorescence intensity within AD300 cells, based on the outcomes shown in Figure 17 (data presented as mean  $\pm$  standard deviation, number of cells counted = 30, \* $p = < 0.001$ ).

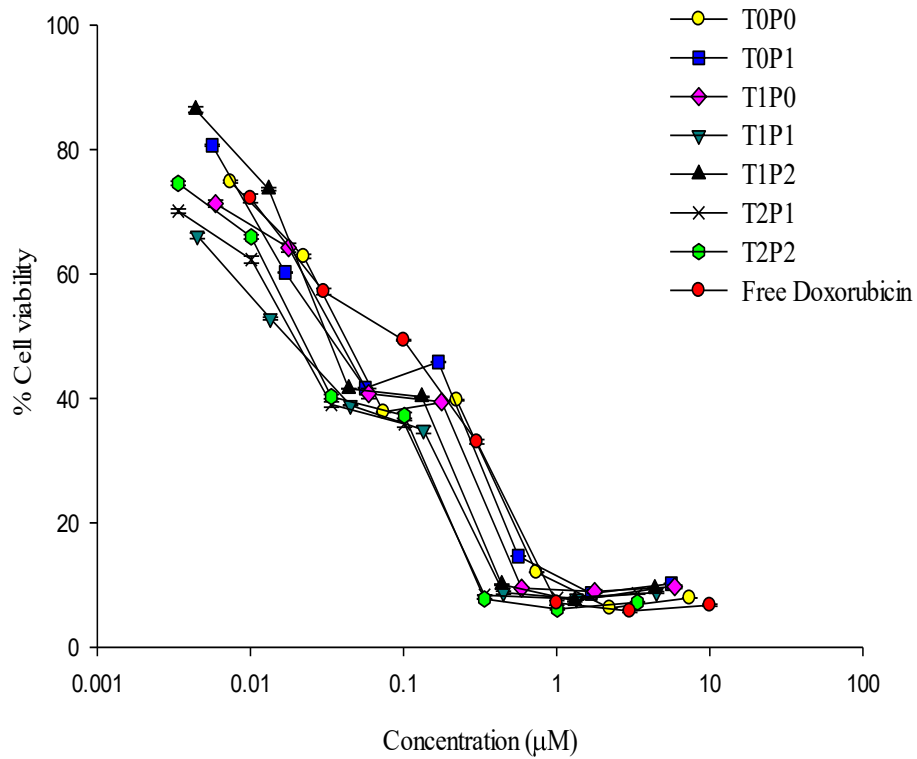


Figure 19: Concentration dependent cytotoxicity profile obtained after treating SW620 cell lines with various doxorubicin-loaded PBCA-NPDS in comparison with free doxorubicin. Data presented as mean  $\pm$  standard deviation, and representative of three independent experiments in triplicate are shown.

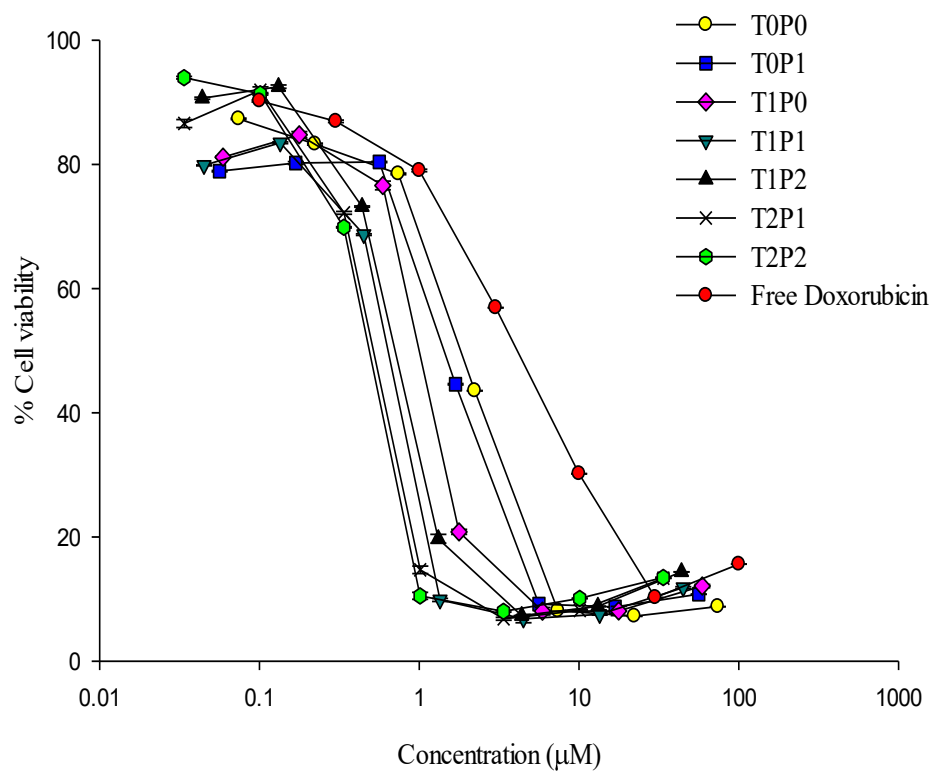


Figure 20: Concentration dependent cytotoxicity profile obtained after treating AD300 cell line with various doxorubicin-loaded PBCA-NPDS in comparison with free doxorubicin. Data presented as mean  $\pm$  standard deviation, and representative of three independent experiments in triplicate are shown.



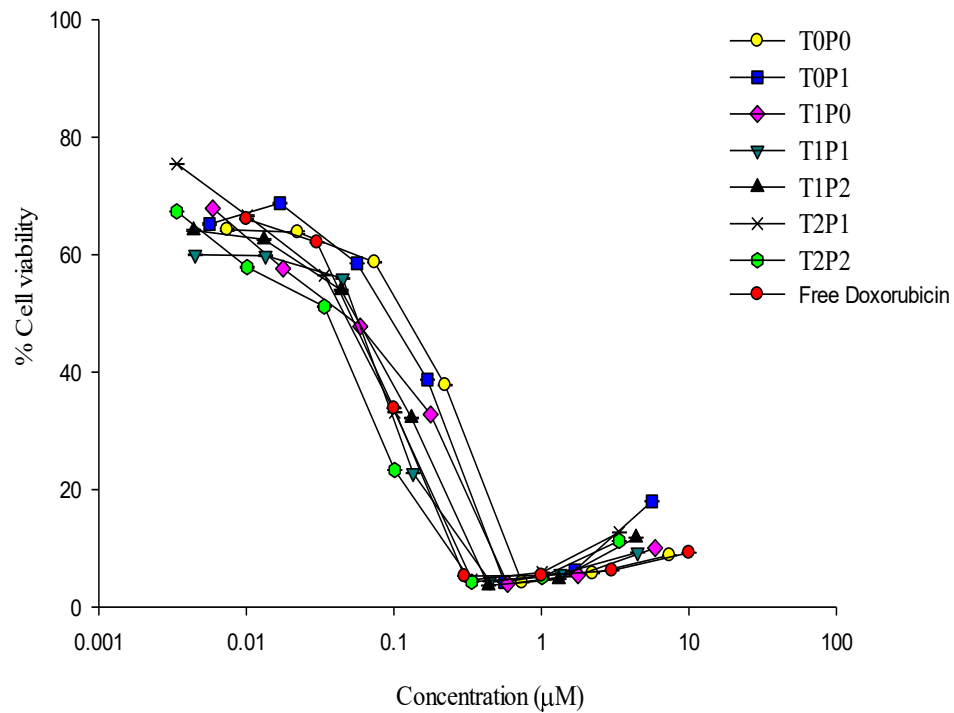


Figure 21: Concentration dependent cytotoxicity profile obtained after treating H460 cell line with various doxorubicin-loaded PBCA-NPDS in comparison with free doxorubicin. Data presented as mean  $\pm$  standard deviation, and representative of three independent experiments in triplicate are shown.

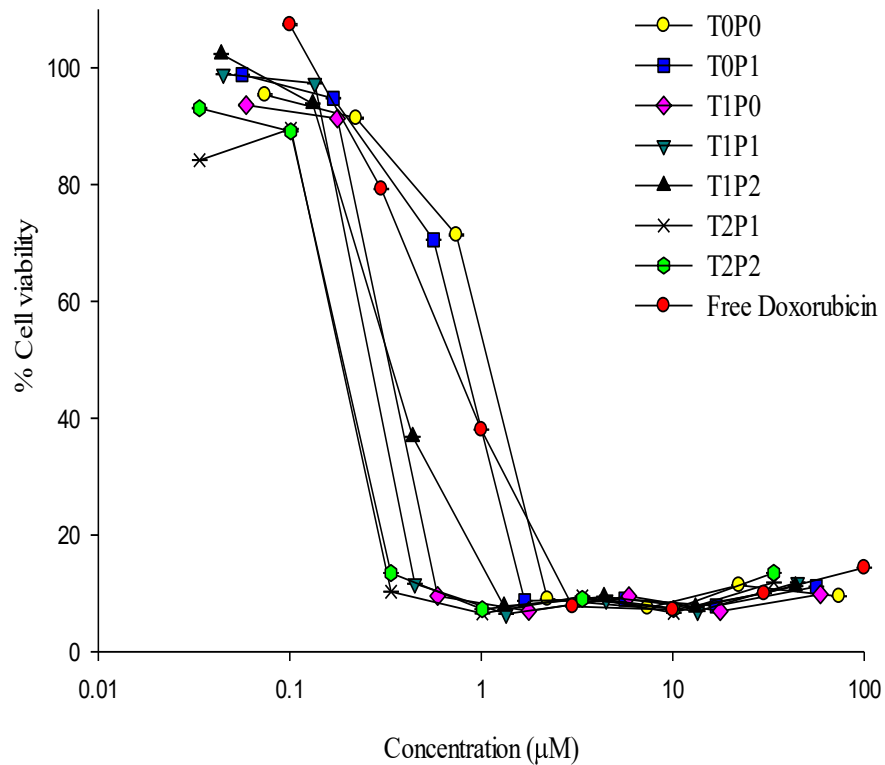


Figure 22: Concentration dependent cytotoxicity profile obtained after treating MX20 cell line with various doxorubicin-loaded PBCA-NPDS in comparison with free doxorubicin. Data presented as mean  $\pm$  standard deviation, and representative of three independent experiments in triplicate are shown.

## 9. References

1. Wu R-Q, Zhang D-F, Tu E, Chen Q-M, Chen W. The mucosal immune system in the oral cavity-an orchestra of T cell diversity. *Int J Oral Sci.* 2014 Sep;6(3):125–32.
2. Pardridge WM. CNS drug design based on principles of blood-brain barrier transport. *J Neurochem.* 1998 May;70(5):1781–92.
3. Greene C, Campbell M. Tight junction modulation of the blood brain barrier: CNS delivery of small molecules. *Tissue barriers.* 4(1):e1138017.
4. Pardridge WM, Buciak JL, Friden PM. Selective transport of an anti-transferrin receptor antibody through the blood-brain barrier in vivo. *J Pharmacol Exp Ther.* 1991 Oct;259(1):66–70.
5. Zhou X, Huang L. Targeted delivery of DANN by liposomes and polymers. *J Control Release.* 1992;19:269–74.
6. Das D, Lin S. Double-Coated Poly (Butylcyanoacrylate) Nanoparticulate Delivery Systems for Brain Targeting of Dalargin Via Oral Administration. *J Pharm Sci.* 2005 Jun;94(6):1343–53.
7. Kreuter J. Drug delivery to the central nervous system by polymeric nanoparticles: What do we know? *Adv Drug Deliv Rev.* 2014 May 1;71:2–14.
8. Kreuter J, Gelperina S. Use of nanoparticles for cerebral cancer. *Tumori J.* 94(2):271–7.
9. Reimold I, Domke D, Bender J, Seyfried CA, Radunz H-E, Fricker G. Delivery of nanoparticles to the brain detected by fluorescence microscopy. *Eur J Pharm Biopharm.* 2008 Oct;70(2):627–32.

10. Ramge P, Kreuter J, Lemmer B. Circadian phase-dependent antinociceptive reaction in mice determined by the hot-plate test and the tail-flick test after intravenous injection of dalargin-loaded nanoparticles. *Chronobiol Int.* 1999 Nov;16(6):767–77.
11. Schroeder U, Sommerfeld P, Sabel BA. Efficacy of oral dalargin-loaded nanoparticle delivery across the blood- brain barrier. *Peptides.* 1998;19(4):777–80.
12. Calvo P, Gouritin B, Chacun H, Desmaële D, D'Angelo J, Noel JP, et al. Long-circulating PEGylated polycyanoacrylate nanoparticles as new drug carrier for brain delivery. *Pharm Res.* 2001 Aug;18(8):1157–66.
13. Gessner A, Olbrich C, Schröder W, Kayser O, Müller RH. The role of plasma proteins in brain targeting: species dependent protein adsorption patterns on brain-specific lipid drug conjugate (LDC) nanoparticles. *Int J Pharm.* 2001 Feb 19;214(1–2):87–91.
14. Kreuter J, Shamenkov D, Petrov V, Ramge P, Cychutek K, Koch-Brandt C, et al. Apolipoprotein-mediated transport of nanoparticle-bound drugs across the blood-brain barrier. *J Drug Target.* 2002 Jun;10(4):317–25.
15. Feng S-S, Chien S. Chemotherapeutic engineering: Application and further development of chemical engineering principles for chemotherapy of cancer and other diseases. *Chem Eng Sci.* 2003 Sep 1;58(18):4087–114.
16. Bromberg L, Alakhov V. Effects of polyether-modified poly(acrylic acid) microgels on doxorubicin transport in human intestinal epithelial Caco-2 cell layers. *J Control Release.* 2003 Feb 14;88(1):11–22.
17. Bellamy WT. P-Glycoproteins and Multidrug Resistance. *Annu Rev*

- Pharmacol Toxicol. 1996;36(1):161–83.
18. Goldstein LJ, Galski H, Fojo A, Willingham M, Lai SL, Gazdar A, et al. Expression of multidrug resistance gene in human cancers. *J Natl Cancer Inst.* 1989;81(2):116–24.
19. Van Zuylen L, Nooter K, Sparreboom A, Verweij J. Development of multidrug-resistance convertors: Sense or nonsense? *Invest New Drugs.* 2000;18(3):205–20.
20. Gelperina SE, Khalansky AS, Skidan IN, Smirnova ZS, Bobruskin AI, Severin SE, et al. Toxicological studies of doxorubicin bound to polysorbate 80-coated poly(butyl cyanoacrylate) nanoparticles in healthy rats and rats with intracranial glioblastoma. *Toxicol Lett.* 2002 Jan 25;126(2):131–41.
21. Dehouck B, Fenart L, Dehouck MP, Pierce A, Torpier G, Cecchelli R. A new function for the LDL receptor: transcytosis of LDL across the blood-brain barrier. *J Cell Biol.* 1997 Aug 25;138(4):877–89.
22. Hosny EA, El-Sayed YM, Al-Meshal MA, Al-Angary AA. Effect of food on bioavailability of bioadhesive-containing indomethacin tablets in dogs. *Int J Pharm.* 1994;112(1):87–91.
23. Lee, Vincent H.L. and Yang JJ. Drug delivery and targeting: Oral Drug Delivery. In: Hillery, Anya M., Lloyd, Andrew W. and Swarbrick J, editor. *Drug delivery and targeting: For pharmacists and pharmaceutical scientists.* NY; 2001. p. 145–82.
24. Lee, Vincent H.L., Dodda-Kashi, Satish, Grass, George M. and Rubas W. Oral route of peptide and protein drug delivery. In: Lee VHL, editor. *Peptide and*

- protein drug delivery. New York: Marcel Dekker Inc.; 1991. p. 691–726.
25. LeFevre ME, Warren JB, Joel DD. Particles and macrophages in murine Peyer's patches. *Exp Cell Biol.* 1985;53(3):121–9.
26. Jani P, Halbert GW, Langridge J, Florence AT. Nanoparticle uptake by the rat gastrointestinal mucosa: quantitation and particle size dependency. *J Pharm Pharmacol.* 1990 Dec;42(12):821–6.
27. Damgé C, Michel C, Aprahamian M, Couvreur P, Devissaguet JP. Nanocapsules as carriers for oral peptide delivery. *J Control Release.* 1990 Aug;13(2–3):233–9.
28. Aprahamian M, Michel C, Humbert W, Devissaguet JP, Damge C. Transmucosal passage of polyalkylcyanoacrylate nanocapsules as a new drug carrier in the small intestine. *Biol cell.* 1987;61(1–2):69–76.
29. Jani P, Halbert GW, Langridge J, Florence AT. The uptake and translocation of latex nanospheres and microspheres after oral administration to rats. *J Pharm Pharmacol.* 1989 Dec;41(12):809–12.
30. PAYNE JM, SANSOM BF, GARNER RJ, THOMSON AR, MILES BJ. Uptake of small resin particles (1-5 microns diameter) by the alimentary canal of the calf. *Nature.* 1960 Nov 12;188:586–7.
31. Volkheimer G. Persorption of particles: physiology and pharmacology. *Adv Pharmacol Chemother.* 1977;14:163–87.
32. SANDERS E, ASHWORTH CT. A study of particulate intestinal absorption and hepatocellular uptake. Use of polystyrene latex particles. *Exp Cell Res.* 1961 Jan;22:137–45.

33. Kreuter J, Müller U, Munz K. Quantitative and microautoradiographic study on mouse intestinal distribution of polycyanoacrylate nanoparticles. *Int J Pharm.* 1989;55(1):39–45.
34. Wolf JL, Bye WA. The membranous epithelial (M) cell and the mucosal immune system. *Annu Rev Med.* 1984;35:95–112.
35. Kreuter J. Peroral administration of nanoparticles. *Adv Drug Deliv Rev.* 1991;7(1):71–86.
36. Scherer D, Mooren FC, Kinne RKH, Kreuter J. In Vitro Permeability of PBCA Nanoparticles through Porcine Small Intestine. *J Drug Target.* 1993 Jan 28;1(1):21–7.
37. Jani PU, Florence AT, McCarthy DE. Further histological evidence of the gastrointestinal absorption of polystyrene nanospheres in the rat. *Int J Pharm.* 1992 Aug;84(3):245–52.
38. Komuro T. Fenestrations of the basal lamina of intestinal villi of the rat. *Cell Tissue Res.* 1985 Jan;239(1):183–8.
39. Tso P, Balint JA. Formation and transport of chylomicrons by enterocytes to the lymphatics. *Am J Physiol.* 1986 Jun;250(6 Pt 1):G715-26.
40. Bearer EL, Orci L. Endothelial fenestral diaphragms: a quick-freeze, deep-etch study. *J Cell Biol.* 1985 Feb;100(2):418–28.
41. Kreuter J. Application of nanoparticles for the delivery of drugs to the brain. *Int Congr Ser.* 2005 Apr;1277:85–94.
42. Kreuter J. Influence of chronobiology on the nanoparticle-mediated drug uptake into the brain. *Pharmaceutics.* 2015 Feb 3;7(1):3–9.

43. Kreuter J. Mechanism of polymeric nanoparticle-based drug transport across the blood-brain barrier (BBB). *J Microencapsul.* 2013;30(1):49–54.
44. Zensi A, Begley D, Pontikis C, Legros C, Mihoreanu L, Wagner S, et al. Albumin nanoparticles targeted with Apo E enter the CNS by transcytosis and are delivered to neurones. *J Control Release.* 2009 Jul;137(1):78–86.
45. Alyaudtin RN, Reichel A, Löbenberg R, Ränge P, Kreuter J, Begley DJ. Interaction of Poly(butylcyanoacrylate) Nanoparticles with the Blood-Brain Barrier in vivo and in vitro. *J Drug Target.* 2001 Jan 8;9(3):209–21.
46. Borchard G, Audus KL, Shi F, Kreuter J. Uptake of surfactant-coated poly(methyl methacrylate)-nanoparticles by bovine brain microvessel endothelial cell monolayers. *Int J Pharm.* 1994 Sep;110(1):29–35.
47. Ränge P, Unger RE, Oltrogge JB, Zenker D, Begley D, Kreuter J, et al. Polysorbate-80 coating enhances uptake of polybutylcyanoacrylate (PBCA)-nanoparticles by human and bovine primary brain capillary endothelial cells. *Eur J Neurosci.* 2000 Jun;12(6):1931–40.
48. Petri B, Bootz A, Khalansky A, Hekmatara T, Müller R, Uhl R, et al. Chemotherapy of brain tumour using doxorubicin bound to surfactant-coated poly(butyl cyanoacrylate) nanoparticles: Revisiting the role of surfactants. *J Control Release.* 2007 Jan;117(1):51–8.
49. Kreuter J, Shamenkov D, Petrov V, Ränge P, Cychutek K, Koch-Brandt C, et al. Apolipoprotein-mediated Transport of Nanoparticle-bound Drugs Across the Blood-Brain Barrier. *J Drug Target.* 2002 Jan 30;10(4):317–25.
50. Kreuter J. Nanoparticulate systems for brain delivery of drugs. *Adv Drug Deliv*



Rev. 2001 Mar;47(1):65–81.

51. Wohlfart S, Gelperina S, Kreuter J. Transport of drugs across the blood–brain barrier by nanoparticles. *J Control Release*. 2012 Jul;161(2):264–73.

52. Kreuter J. Mechanism of polymeric nanoparticle-based drug transport across the blood-brain barrier (BBB). *J Microencapsul*. 2013 Feb 7;30(1):49–54.

53. Michaelis K. Covalent Linkage of Apolipoprotein E to Albumin Nanoparticles Strongly Enhances Drug Transport into the Brain. *J Pharmacol Exp Ther*. 2006 Mar 2;317(3):1246–53.

54. Kreuter J, Hekmatara T, Dreis S, Vogel T, Gelperina S, Langer K. Covalent attachment of apolipoprotein A-I and apolipoprotein B-100 to albumin nanoparticles enables drug transport into the brain. *J Control Release*. 2007 Mar;118(1):54–8.

55. Panzenboeck U, Balazs Z, Sovic A, Hrzenjak A, Levak-Frank S, Wintersperger A, et al. ABCA1 and Scavenger Receptor Class B, Type I, Are Modulators of Reverse Sterol Transport at an in Vitro Blood-Brain Barrier Constituted of Porcine Brain Capillary Endothelial Cells. *J Biol Chem*. 2002 Nov 8;277(45):42781–9.

56. Balazs Z, Panzenboeck U, Hammer A, Sovic A, Quehenberger O, Malle E, et al. Uptake and transport of high-density lipoprotein (HDL) and HDL-associated  $\alpha$ -tocopherol by an in vitro blood-brain barrier model. *J Neurochem*. 2004;89(4):939–50.

57. Wohlfart S, Gelperina S, Kreuter J. Transport of drugs across the blood-brain barrier by nanoparticles. *J Control Release*. 2012 Jul 20;161(2):264–73.

58. Couvreur P, Kante B, Roland M, Guiot P, Bauduin P, Speiser P. Polycyanoacrylate nanocapsules as potential lysosomotropic carriers: preparation, morphological and sorptive properties. *J Pharm Pharmacol*. 1979 May;31(5):331–2.
59. Leonard F, Kulkarni RK, Brandes G, Nelson J, Cameron JJ. Synthesis and degradation of poly (alkyl  $\alpha$ -cyanoacrylates). *J Appl Polym Sci*. 1966 Feb;10(2):259–72.
60. King ME, Kinney AY. Tissue adhesives: a new method of wound repair. *J Nurse Pr*. 1999 Oct;24(10):66, 69–70, 73–4.
61. Oowaki H, Matsuda S, Sakai N, Ohta T, Iwata H, Sadato A, et al. Non-adhesive cyanoacrylate as an embolic material for endovascular neurosurgery. *Biomaterials*. 2000 May;21(10):1039–46.
62. Reece TB, Maxey TS, Kron IL. A prospectus on tissue adhesives. *Am J Surg*. 2001 Aug;182(2 Suppl):40S-44S.
63. Pollak JS, White RI. The use of cyanoacrylate adhesives in peripheral embolization. *J Vasc Interv Radiol*. 2001 Aug;12(8):907–13.
64. Ravi Kumar MN. Nano and microparticles as controlled drug delivery devices. *J Pharm Pharm Sci*. 2000;3(2):234–58.
65. Soppimath KS, Aminabhavi TM, Kulkarni AR, Rudzinski WE. Biodegradable polymeric nanoparticles as drug delivery devices. *J Control Release*. 2001 Jan;70(1–2):1–20.
66. Couvreur P, Barratt G, Fattal E, Legrand P, Vauthier C. Nanocapsule technology: a review. *Crit Rev Ther Drug Carrier Syst*. 2002;19(2):99–134.

67. Brigger I, Dubernet C, Couvreur P. Nanoparticles in cancer therapy and diagnosis. *Adv Drug Deliv Rev.* 2012;64(SUPPL.):24–36.
68. Stella B, Arpicco S, Peracchia MT, Desmaële D, Hoebeke J, Renoir M, et al. Design of folic acid-conjugated nanoparticles for drug targeting. *J Pharm Sci.* 2000 Nov;89(11):1452–64.
69. Brigger I, Chaminade P, Marsaud V, Appel M, Besnard M, Gurny R, et al. Tamoxifen encapsulation within polyethylene glycol-coated nanospheres. A new antiestrogen formulation. *Int J Pharm.* 2001 Feb 19;214(1–2):37–42.
70. El Egeakey MA, Speiser P. Drug loading studies on ultrafine solid carriers by sorption procedures. *Pharm Acta Helv.* 1982;57(8):236–40.
71. Maincent P, Devissaguet JP, LeVerge R, Sado PA, Couvreur P. Preparation and in vivo studies of a new drug delivery system. *Appl Biochem Biotechnol.* 1984 Feb;10(1–3):263–5.
72. Douglas SJ, Davis SS, Holding SR. Molecular weights of poly(butyl 2-cyanoacrylate) produced during nanoparticle formation. *Br Polym J.* 1985 Dec;17(4):339–42.
73. Bentele V, Berg UE, Kreuter J. Molecular weights of poly ( methyl methacrylate ) nanoparticles. *Int J Pharm.* 1983;109–13.
74. Douglas S., Illum L, Davis S., Kreuter J. Particle size and size distribution of poly(butyl-2-cyanoacrylate) nanoparticles. *J Colloid Interface Sci.* 1984 Sep;101(1):149–58.
75. Douglas S., Illum L, Davis S. Particle size and size distribution of poly(butyl 2-cyanoacrylate) nanoparticles. II. Influence of stabilizers. *J Colloid Interface Sci.*

1985 Jan;103(1):154–63.

76. Birrenbach G, Speiser PP. Polymerized micelles and their use as adjuvants in immunology. *J Pharm Sci.* 1976 Dec;65(12):1763–6.

77. Ekman B, Loftler C, Sjöholm I. Incorporation of macromolecules in microparticles: preparation and characteristics. *Biochemistry.* 1976 Nov 16;15(23):5115–20.

78. Ekman B, Sjöholm I. Improved Stability of Proteins Immobilized in Microparticles Prepared by a Modified Emulsion Polymerization Technique. *J Pharm Sci.* 1978 May;67(5):693–6.

79. Krause H-J, Schwarz A, Rohdewald P. Interfacial Polymerization, A Useful Method for the Preparation of Polymethylcyanoacrylate Nanoparticles. *Drug Dev Ind Pharm.* 1986 Jan 20;12(4):527–52.

80. Al Khouri Fallouh N, Roblot-Treupel L, Fessi H, Devissaguet JP, Puisieux F. Development of a new process for the manufacture of polyisobutylcyanoacrylate nanocapsules. *Int J Pharm.* 1986 Feb;28(2–3):125–32.

81. Chouinard F, Kan FWK, Leroux J-C, Foucher C, Lenaerts V. Preparation and purification of polyisohexylcyanoacrylate nanocapsules. *Int J Pharm.* 1991 Jun;72(3):211–7.

82. Tobío, Sánchez, Vila, Soriano, Evora, Vila-Jato, et al. The role of PEG on the stability in digestive fluids and in vivo fate of PEG-PLA nanoparticles following oral administration. *Colloids Surf B Biointerfaces.* 2000 Oct 1;18(3–4):315–23.

83. Klibanov AL, Maruyama K, Torchilin VP, Huang L. Amphipathic polyethyleneglycols effectively prolong the circulation time of liposomes. *FEBS*

Lett. 1990 Jul 30;268(1):235–7.

84. Blume G, Cevc G. Liposomes for the sustained drug release in vivo. *Biochim Biophys Acta*. 1990 Nov 2;1029(1):91–7.

85. Woodle MC, Lasic DD. Sterically stabilized liposomes. *Biochim Biophys Acta*. 1992 Aug 14;1113(2):171–99.

86. Torchilin VP, Papisov MI. Why do Polyethylene Glycol-Coated Liposomes Circulate So Long?: Molecular Mechanism of Liposome Steric Protection with Polyethylene Glycol: Role of Polymer Chain Flexibility. *J Liposome Res*. 1994 Jan 28;4(1):725–39.

87. Jeon S., Lee J., Andrade J., De Gennes P. Protein—surface interactions in the presence of polyethylene oxide. *J Colloid Interface Sci*. 1991 Mar;142(1):149–58.

88. Jeon S., Andrade J. Protein—surface interactions in the presence of polyethylene oxide. *J Colloid Interface Sci*. 1991 Mar;142(1):159–66.

89. Muir IS, Moghimi SM, Illum L, Davis SS, Davies MC. The effect of block copolymers on the uptake of model polystyrene microspheres by Kupffer cells--in vitro and in vivo studies. *Biochem Soc Trans*. 1991 Aug;19(3):329S.

90. Gullikson GW, Cline WS, Lorenzsonn V, Benz L, Olsen WA, Bass P. Effects of anionic surfactants on hamster small intestinal membrane structure and function: relationship to surface activity. *Gastroenterology*. 1977 Sep;73(3):501–11.

91. Eyles J, Alpar O, Field WN, Lewis DA, Keswick M. The transfer of polystyrene microspheres from the gastrointestinal tract to the circulation after oral administration in the rat. *J Pharm Pharmacol*. 1995 Jul;47(7):561–5.

92. LeFevre ME, Hancock DC, Joel DD. Intestinal barrier to large particulates in mice. *J Toxicol Environ Health*. 1980 Jul 15;6(4):691–704.
93. Greenwald RB. PEG drugs: An overview. *J Control Release*. 2001;74(1–3):159–71.
94. Kreuter J. Physicochemical characterization of polyacrylic nanoparticles. *Int J Pharm*. 1983 Mar;14(1):43–58.
95. Kreuter J. On the mechanism of termination in heterogeneous polymerization. *J Polym Sci Polym Lett Ed*. 1982 Oct;20(10):543–5.
96. El-Egakey M. Molecular weights of polycyanoacrylate nanoparticles. *Int J Pharm*. 1983 Feb;13(3):349–52.
97. Fouarge M, Dewulft M, Couvreur P, Roland M, Vranckx H. Development of dehydroemetine nanoparticles for the treatment of visceral leishmaniasis. *J Microencapsul*. 1989 Jan 27;6(1):29–34.
98. Gedde UW. Thermal Analysis of Polymers. In: *Polymer Physics*. Dordrecht: Springer Netherlands; 1999. p. 217–37.
99. Benoit JP, Benita S, Puisieux F, Thies C. Stability and release kinetics of drugs incorporated within microspheres. In: *Microspheres and Drug Therapy Pharmaceutical, Immunological and Medical Aspects*. Elsevier Amsterdam; 1984. p. 91–102.
100. Yalabik-Kas HS, Kreuter J, Hincal AA, Speiser PP. Sorption of 5-fluorouracil from aqueous solutions onto methyl methacrylate nanoparticles. *J Microencapsul*. 1986 Jan 27;3(2):71–5.
101. Tröster SD, Kreuter J. Contact angles of surfactants with a potential to alter

- the body distribution of colloidal drug carriers on poly (methyl methacrylate) surfaces. *Int J Pharm.* 1988 Jul;45(1-2):91-100.
102. Carstensen H, Müller BW, Müller RH. Adsorption of ethoxylated surfactants on nanoparticles. I. Characterization by hydrophobic interaction chromatography. *Int J Pharm.* 1991 Jan;67(1):29-37.
103. Tröster SD, Wallis KH, Müller RH, Kreuter J. Correlation of the surface hydrophobicity of <sup>14</sup>C-poly(methyl methacrylate) nanoparticles to their body distribution. *J Control Release.* 1992 Aug;20(3):247-60.
104. Kulkarni RK, Hanks GA, Pani KC, Leonard F. Their *vivo* metabolic degradation of poly (methyl cyanoacrylate) via thiocyanate. *J Biomed Mater Res.* 1967 Mar;1(1):11-6.
105. Mori S, Ota K, Takada M, Inou T. Comparative studies of cyanoacrylate derivatives *in vivo*. *J Biomed Mater Res.* 1967 Mar;1(1):55-65.
106. Vezin WR, Florence AT. *In Vitro* Degradation Rates of Biodegradable Poly-N-Alkyl Cyanoacrylates. *J Pharm Pharmacol.* 1978;30(S1):5P-5P.
107. Lenaerts V, Couvreur P, Christiaens-Leyh D, Joiris E, Roland M, Rollman B, et al. Degradation of poly (isobutyl cyanoacrylate) nanoparticles. *Biomaterials.* 1984 Mar;5(2):65-8.
108. Youssef M, Fattal E, Alonso MJ, Roblot-Treupel L, Sauzières J, Tancredi C, et al. Effectiveness of nanoparticle-bound ampicillin in the treatment of *Listeria monocytogenes* infection in athymic nude mice. *Antimicrob Agents Chemother.* 1988 Aug;32(8):1204-7.
109. Chavany C, Doan T Le, Couvreur P, Puisieux F, Hélène C.

Polyalkylcyanoacrylate Nanoparticles as Polymeric Carriers for Antisense Oligonucleotides. *Pharm Res.* 1992 Apr;9(4):441–9.

110. Kreuter, J., Mills, S., N., Davis, S. S., Wilson CG. Polybutylcyanoacrylate nanoparticles for the delivery of [<sup>75</sup>Se] norcholesterol. *Int J Pharm.* 1983;106:105–13.

111. Couvreur P, Kante B, Roland M, Speiser P. Adsorption of antineoplastic drugs to polyalkylcyanoacrylate nanoparticles and their release in calf serum. *J Pharm Sci.* 1979 Dec;68(12):1521–4.

112. Harmia T, Kreuter J, Speiser P, Boye T, Gurny R, Kubi A. Enhancement of the myotic response of rabbits with pilocarpine-loaded polybutylcyanoacrylate nanoparticles. *Int J Pharm.* 1986 Nov;33(1–3):187–93.

113. el-Samaligy MS, Rohdewald P, Mahmoud HA. Polyalkyl cyanoacrylate nanocapsules. *J Pharm Pharmacol.* 1986 Mar;38(3):216–8.

114. Malaiya A, Vyas SP. Preparation and characterization of indomethacin magnetic nanoparticles. *J Microencapsul.* 1988 Jan 27;5(3):243–53.

115. Cappel MJ, Kreuter J. Effect of nanoparticles on transdermal drug delivery. *J Microencapsul.* 1991 Jan 27;8(3):369–74.

116. Seijo B, Fattal E, Roblot-Treupel L, Couvreur P. Design of nanoparticles of less than 50 nm diameter: preparation, characterization and drug loading. *Int J Pharm.* 1990;62(1):1–7.

117. El-Samaligy M, Rohdewald P. Triamcinolone diacetate nanoparticles, a sustained release drug delivery system suitable for parenteral administration. *Pharm Acta Helv.* 1982;57(7):201–4.



118. Wu DC, Ofner CM. Adsorption and Degradation of Doxorubicin from Aqueous Solution in Polypropylene Containers. *AAPS PharmSciTech*. 2013 Mar 11;14(1):74–7.
119. Klein S. The use of biorelevant dissolution media to forecast the in vivo performance of a drug. *AAPS J*. 2010 Sep;12(3):397–406.
120. Wang X, Hui R, Chen Y, Wang W, Chen Y, Gong X, et al. Discovery of Novel Doxorubicin Metabolites in MCF7 Doxorubicin-Resistant Cells. *Front Pharmacol*. 2019;10:1434.
121. Kauffman M, Kauffman M, Zhu H, Jia Z, Li Y. Fluorescence-Based Assays for Measuring Doxorubicin in Biological Systems. *React Oxy Species*. 2016;
122. Zhou Q, Chowbay B. Determination of doxorubicin and its metabolites in rat serum and bile by LC: application to preclinical pharmacokinetic studies. *J Pharm Biomed Anal*. 2002 Nov;30(4):1063–74.
123. Zhang Y-K, Zhang G-N, Wang Y-J, Patel BA, Talele TT, Yang D-H, et al. Bafetinib (INNO-406) reverses multidrug resistance by inhibiting the efflux function of ABCB1 and ABCG2 transporters. *Sci Rep*. 2016;6(1):25694.
124. Kreuter J, Alyautdin RN, Kharkevich DA, Ivanov AA. Passage of peptides through the blood-brain barrier with colloidal polymer particles (nanoparticles). *Brain Res*. 1995 Mar 13;674(1):171–4.
125. Zradni F-Z, Hamelin J, Derdour A. Synthesis of amides from esters and amines under microwave irradiation. *Synth Commun*. 2002;32(22):3525–31.
126. Mielczarek-Putka M, Struga M, Roszkowski P. Synthesis and anticancer effects of conjugates of doxorubicin and unsaturated fatty acids (LNA and DHA).

Med Chem Res. 2019;28(12):2153–64.

127. Ramesh P, Fadnavis NW. Ammonium Nitrate: A Biodegradable and Efficient Catalyst for the Direct Amidation of Esters under Solvent-free Conditions. Chem Lett. 2015 Feb 5;44(2):138–40.

128. Papadimitriou S, Bikiaris D. Novel self-assembled core-shell nanoparticles based on crystalline amorphous moieties of aliphatic copolyesters for efficient controlled drug release. J Control Release. 2009 Sep 1;138(2):177–84.

129. Shah MK, Madan P, Lin S. Preparation, in vitro evaluation and statistical optimization of carvedilol-loaded solid lipid nanoparticles for lymphatic absorption via oral administration. Pharm Dev Technol. 2014;19(4):475–85.

130. Solomon D, Gupta N, Mulla NS, Shukla S, Guerrero YA, Gupta V. Role of In Vitro Release Methods in Liposomal Formulation Development: Challenges and Regulatory Perspective. AAPS J. 2017 Nov 18;19(6):1669–81.

131. D'Souza S. A Review of In Vitro Drug Release Test Methods for Nano-Sized Dosage Forms . Adv Pharm. 2014;2014:1–12.

132. Kutlehria S, Behl G, Patel K, Doddapaneni R, Vhora I, Chowdhury N, et al. Cholecalciferol-PEG Conjugate Based Nanomicelles of Doxorubicin for Treatment of Triple-Negative Breast Cancer. AAPS PharmSciTech. 2018 Feb 10;19(2):792–802.

133. Boakye CHA, Patel K, Singh M. Doxorubicin liposomes as an investigative model to study the skin permeation of nanocarriers. Int J Pharm. 2015 Jul;489(1–2):106–16.

134. Xu X, Khan MA, Burgess DJ. A two-stage reverse dialysis in vitro

- dissolution testing method for passive targeted liposomes. *Int J Pharm.* 2012 Apr;426(1–2):211–8.
135. Yu M, Yuan W, Li D, Schwendeman A, Schwendeman SP. Predicting drug release kinetics from nanocarriers inside dialysis bags. *J Control Release.* 2019;315:23–30.
136. Furuichi K, Ra C, Isersky C, Rivera J. Comparative evaluation of the effect of pharmacological agents on endocytosis and coendocytosis of IgE by rat basophilic leukaemia cells. *Immunology.* 1986 May;58(1):105–10.
137. Martins AS, Ordóñez JL, Amaral AT, Prins F, Floris G, Debiec-Rychter M, et al. IGF1R Signaling in Ewing Sarcoma Is Shaped by Clathrin-/Caveolin-Dependent Endocytosis. Srivastava RK, editor. *PLoS One.* 2011 May 17;6(5):e19846.
138. Wagner S, Zensi A, Wien SL, Tschickardt SE, Maier W, Vogel T, et al. Uptake Mechanism of ApoE-Modified Nanoparticles on Brain Capillary Endothelial Cells as a Blood-Brain Barrier Model. Deli MA, editor. *PLoS One.* 2012 Mar 1;7(3):e32568.
139. Ritter P, Yousefi K, Ramirez J, Dykxhoorn DM, Mendez AJ, Shehadeh LA. LDL Cholesterol Uptake Assay Using Live Cell Imaging Analysis with Cell Health Monitoring. *J Vis Exp.* 2018 Nov 17;(141).
140. Ashfaq UA, Javed T, Rehman S, Nawaz Z, Riazuddin S. Lysosomotropic agents as HCV entry inhibitors. *Virol J.* 2011 Dec 12;8(1):163.
141. Zhang Y-K, Zhang H, Zhang G-N, Wang Y-J, Kathawala RJ, Si R, et al. Semi-synthetic ocotillol analogues as selective ABCB1-mediated drug resistance

- reversal agents. *Oncotarget*. 2015 Sep 15;6(27):24277–90.
142. Neves AR, Queiroz JF, Lima SAC, Reis S. Apo E-Functionalization of Solid Lipid Nanoparticles Enhances Brain Drug Delivery: Uptake Mechanism and Transport Pathways. *Bioconjug Chem*. 2017 Apr 19;28(4):995–1004.
143. Brown RC, Morris AP, O’Neil RG. Tight junction protein expression and barrier properties of immortalized mouse brain microvessel endothelial cells. *Brain Res*. 2007 Jan;1130:17–30.
144. Jensen EC. Quantitative Analysis of Histological Staining and Fluorescence Using ImageJ. *Anat Rec*. 2013 Mar;296(3):378–81.
145. Cázares-Delgadillo J, Balaguer-Fernandez C, Calatayud-Pascual A, Ganem-Rondero A, Quintanar-Guerrero D, Lopez-Castellano AC, et al. Transdermal iontophoresis of dexamethasone sodium phosphate in vitro and in vivo: effect of experimental parameters and skin type on drug stability and transport kinetics. *Eur J Pharm Biopharm*. 2010;75(2):173–8.
146. Vansnick L, Couvreur P, Christiaens-Leyh D, Roland M. Molecular Weights of Free and Drug-Loaded Nanoparticles. *Pharm Res*. 1985;2(1):36–41.
147. Chognot D, Six JL, Leonard M, Bonneaux F, Vigneron C, Dellacherie E. Physicochemical evaluation of PLA nanoparticles stabilized by water-soluble MPEO–PLA block copolymers. *J Colloid Interface Sci*. 2003 Dec;268(2):441–7.
148. Tejwani RW, Joshi HN, Varia SA, Serajuddin ATM. Study of Phase Behavior of Poly(ethylene glycol)–Polysorbate 80 and Poly(ethylene glycol)–Polysorbate 80–Water Mixtures. *J Pharm Sci*. 2000 Jul;89(7):946–50.
149. Danaei M, Dehghankhold M, Ataei S, Hasanzadeh Davarani F, Javanmard R,

- Dokhani A, et al. Impact of Particle Size and Polydispersity Index on the Clinical Applications of Lipidic Nanocarrier Systems. *Pharmaceutics*. 2018 May 18;10(2):57.
150. Duffy C, Zetterlund P, Aldabbagh F. Radical Polymerization of Alkyl 2-Cyanoacrylates. *Molecules*. 2018 Feb 20;23(2):465.
151. Kreuter J. Nanoparticles. In: *Colloidal Drug Delivery Systems*. New York: Marcel Dekker Inc.; 1994. p. 277–8.
152. Ke X, Coady DJ, Yang C, Engler AC, Hedrick JL, Yang YY. pH-sensitive polycarbonate micelles for enhanced intracellular release of anticancer drugs: a strategy to circumvent multidrug resistance. *Polym Chem*. 2014;5(7):2621–8.
153. Gref R, Lück M, Quellec P, Marchand M, Dellacherie E, Harnisch S, et al. ‘Stealth’ corona-core nanoparticles surface modified by polyethylene glycol (PEG): influences of the corona (PEG chain length and surface density) and of the core composition on phagocytic uptake and plasma protein adsorption. *Colloids Surfaces B Biointerfaces*. 2000 Oct;18(3–4):301–13.
154. Suk JS, Xu Q, Kim N, Hanes J, Ensign LM. PEGylation as a strategy for improving nanoparticle-based drug and gene delivery. *Adv Drug Deliv Rev*. 2016 Apr;99:28–51.
155. Le Roy C, Wrana JL. Clathrin- and non-clathrin-mediated endocytic regulation of cell signalling. *Nat Rev Mol Cell Biol*. 2005 Feb;6(2):112–26.
156. Tahara K, Sakai T, Yamamoto H, Takeuchi H, Hirashima N, Kawashima Y. Improved cellular uptake of chitosan-modified PLGA nanospheres by A549 cells. *Int J Pharm*. 2009 Dec;382(1–2):198–204.

157. Carvalho C, Santos R, Cardoso S, Correia S, Oliveira P, Santos M, et al. Doxorubicin: The Good, the Bad and the Ugly Effect. *Curr Med Chem*. 2009 Sep 1;16(25):3267–85.
158. Hillaireau H, Couvreur P. Nanocarriers' entry into the cell: relevance to drug delivery. *Cell Mol Life Sci*. 2009 Sep 5;66(17):2873–96.
159. Petros RA, DeSimone JM. Strategies in the design of nanoparticles for therapeutic applications. *Nat Rev Drug Discov*. 2010 Aug 9;9(8):615–27.
160. Hoosain FG, Choonara YE, Tomar LK, Kumar P, Tyagi C, du Toit LC, et al. Bypassing P-Glycoprotein Drug Efflux Mechanisms: Possible Applications in Pharmaco-resistant Schizophrenia Therapy. *Biomed Res Int*. 2015;2015:1–21.
161. Lenaerts V, Nagelkerke JF, Van Berkel TJC, Couvreur P, Grislain L, Roland M, et al. In Vivo Uptake of Polyisobutyl Cyanoacrylate Nanoparticles by Rat Liver Kupffer, Endothelial, and Parenchymal Cells. *J Pharm Sci*. 1984 Jul;73(7):980–2.
162. Pinto-Alphandary H, Balland O, Laurent M, Andremont A, Puisieux F, Couvreur P. Intracellular Visualization of Ampicillin-Loaded Nanoparticles in Peritoneal Macrophages Infected in Vitro with *Salmonella typhimurium*. *Pharm Res*. 1994;11(1):38–46.
163. Khan Z, Bagad M. Poly(n-butylcyanoacrylate) nanoparticles for oral delivery of quercetin: preparation, characterization, and pharmacokinetics and biodistribution studies in Wistar rats. *Int J Nanomedicine*. 2015 Jun;3921.
164. Yordanov G. Influence of the preparation method on the physicochemical properties of econazole-loaded poly(butyl cyanoacrylate) colloidal nanoparticles. *Colloids Surfaces A Physicochem Eng Asp*. 2012 Nov;413:260–5.

165. Brocks DR, Davies NM. Lymphatic Drug Absorption via the Enterocytes: Pharmacokinetic Simulation, Modeling, and Considerations for Optimal Drug Development. *J Pharm Pharm Sci*. 2018 Oct 23;21(1s):254s-270s.
166. Liao D, Zhang W, Gupta P, Lei Z-N, Wang J-Q, Cai C-Y, et al. Tetrandrine Interaction with ABCB1 Reverses Multidrug Resistance in Cancer Cells Through Competition with Anti-Cancer Drugs Followed by Downregulation of ABCB1 Expression. *Molecules*. 2019 Nov 30;24(23):4383.
167. Petkova V, Benattar J-J, Zoonens M, Zito F, Popot J-L, Polidori A, et al. Free-standing films of fluorinated surfactants as 2D matrices for organizing detergent-solubilized membrane proteins. *Langmuir*. 2007 Apr 10;23(8):4303–9.
168. Gref, Lück, Quellec, Marchand, Dellacherie, Harnisch, et al. “Stealth” corona-core nanoparticles surface modified by polyethylene glycol (PEG): influences of the corona (PEG chain length and surface density) and of the core composition on phagocytic uptake and plasma protein adsorption. *Colloids Surf B Biointerfaces*. 2000 Oct 1;18(3–4):301–13.

## Vita

Name	<i>Neeraj Kaushal</i>
Baccalaureate Degree	<i>Bachelor's in pharmacy, Rajiv Gandhi University of Health Sciences, Bangalore, India</i>  <i>Major: Pharmaceutical Sciences</i>
Date Graduated	<i>October 2008</i>
Other Degrees and Certificates	<i>Master of Science, Long Island University, Brooklyn, NY</i>  <i>Major: Chemistry</i>
Date Graduated	<i>August 2012</i>